Coupling strategies for compressible - low Mach number flows

Yohan Penel, Stéphane Dellacherie, Bruno Després

Coupling strategies for compressible – low Mach number flows

Yohan Penel[*] Stéphane Dellacherie[‡] Bruno Després[†]

December 30, 2013

Abstract

In order to enrich the modelling of fluid flows, we investigate in this paper a coupling between two models dedicated to distinct regimes. More precisely, we focus on the influence of the Mach number as the low Mach case is known to induce theoretical and numerical issues in a compressible framework. A moving interface is introduced to separate a compressible model (Euler with source term) and its low Mach counterpart through relevant transmission conditions. A global steady state for the coupled problem is exhibited. Numerical simulations are then performed to highlight the influence of the coupling by means of a robust numerical strategy.

1 Introduction

Numerical simulations of fluid mechanics phenomena are of great interest in the framework of society issues such as the prevention of natural hazards (tsunamis, ...), the design of water-based facilities (nuclear reactors, ...), tests for new medical treatments (modelling of blood, ...) or the quest for new energy sources (water-turbines, ...). Each one of these fluid flows has some specific features (Reynolds number, Mach number, Froude number, ...) corresponding to specific regimes (viscous flows, compressible flows, ...) and requiring specific numerical handlings. Designing an efficient numerical strategy must thus take into account those specific regimes. The resulting code must not only be accurate at the specific conditions it is designed for, but also be robust when flow conditions evolve over a wider range. Indeed, even if standard configurations correspond to small values of a given parameter, the code must be able to cope with unusual situations where this parameter increases dramatically.

In the present work, we focus on Mach-parametrized fluid flows. We recall that the Mach number is the ratio between the flow velocity and the speed of sound. This characteristic number ranges from 0 (*e.g.* incompressible flows) to large values (hypersonic flows) with a large spectrum of quite different behaviours. In particular, the issue of low Mach number flows has long been addressed in the literature. From a theoretical point of view, the formal convergence of solutions to a given compressible (mostly barotropic) model towards solutions to the related incompressible system was proven in the periodic/infinite domain case by Klainerman & Majda [27,28] for well-prepared initial conditions. The

[*]Team ANGE, CEREMA (Ministry of Ecology, Sustainable Development and Energy) and INRIA – Paris-Rocquencourt, Domaine de Voluceau, BP105, F-78153 Le Chesnay Cedex

[†]Sorbonne Universités, UPMC Univ. Paris 06 and CNRS, UMR 7598, Laboratoire Jacques-Louis Lions, F-75005, Paris, France; emails: yohan.penel@gmail.com and despres@ann.jussieu.fr

[‡]DEN/DANS/DM2S/STMF, Commissariat à l'Énergie Atomique et aux Énergies Alternatives – Saclay, F-91191 Gif-sur-Yvette, France; email: stephane.dellacherie@cea.fr

case of general initial conditions was studied by Schochet [42]. The extension to bounded domains was achieved by Desjardins *et al.* [15]. The conclusion drawn in these works is that the initial existence of too large variations of pressure persist and damage the convergence with the Mach number. This inaccuracy also occurs from a numerical point of view [13, 21, 22, 48] where spurious pressure and velocity waves appear. This is not the only specific numerical issue. Indeed, the disparity of orders of magnitude of the Mach number results in a large range of time scales which mainly influences the computations. On the one hand, explicit schemes are over-constrained by an acoustic CFL condition. On the other hand, implicit schemes may help improve efficency without any stability condition but at the expense of accuracy as phenomena at the flow time scale might disappear due to a too large time step.

Several numerical strategies have been proposed to tackle this issue by adapting either compressible or incompressible solvers to the low Mach regime. The latter case essentially consists in deriving an elliptic equation for p [6, 26, 37]. As for compressible solvers, many approaches have been studied: a classical one like in [29] consists in a time splitting method with an implicit treatment of the acoustic part and an explicit one for the material part. In [21, 22], Guillard and his co-workers blame the numerical dissipation of the numerical instabilities at low Mach number. Modifications of standard Riemann solvers are thereby derived through an asymptotic expansion with respect to the Mach number injected into the discrete formulation. In [13], Dellacherie performed an analysis similar to Schochet [42]: relying on the decomposition of differential operators into fast and slow parts, the author compared kernels of continuous and discrete operators. We also mention an intermediate approach [11] where the Hodge decomposition is used to single out the incompressible part within the compressible model and the work of Chalons *et al* [7] where a numerical scheme is designed in an asymptotic-preserving framework.

There are some industrial frameworks where attention is drawn to steady states. Stationary states can be useful to provide information about the system as well as to initialize computations for stability studies. That is why transient states could be less important. Most common techniques to fasten the convergence towards these states rely on preconditioning (see for instance [25, 35, 47] mainly for combustion applications). On the one hand, pseudo-unstationary simulations can be carried out for systems that admit the same steady states as the studied model, with viscous effects [35] or without [47]. On the other hand, the Mach number transformation presented in [25] consists in a change of variables $p \to p - p_{ref}$ where p_{ref} is chosen such that the resulting pressure variable is positive and the speed of sound is lowered in order to relax the time constraint.

The aforementioned approaches to low Mach regimes rely on a modification of standard numerical schemes. A significantly different strategy consists in modifying the equations thanks to an asymptotic expansion with respect to the Mach number. A natural idea would make the compressible model replaced by its incompressible counterpart insofar as it is its (singular) limit. Nevertheless, such models cannot account for large density/temperature variations that are present even for slightly compressible flows. Asymptotic expansions enable to construct a hierarchy of intermediate models (depending on the order of terms that are kept on) that preserve thermodynamic effects. Pioneering works were devoted to the modelling of combustion. See papers from Sivashinsky [45], Majda and co-workers [32,33], where low Mach models were derived. We also mention more recent works in the nuclear framework [4,5,12]. These models are characterized by a filtering out of the acoustic waves [39] whose consequence is the co-existence of two pressure fields. A non-homogeneous divergence constraint replaces the classical energy equation (or the continuity equation). A major consequence is thus the change of nature of the system of PDEs: for instance, the low Mach model derived from the hyperbolic Euler equations is elliptic–hyperbolic as detailed below. The resulting model can then be simulated by means of new numerical strategies. Notice that unsteady solutions of 1D versions of these low Mach number models can often be explicitly expressed [5,45]. More general models are derived in [29] with 1 time / 2 space scales (a third pressure field is then necessary in the modelling) and in [43] with 2 time / 2 space scales

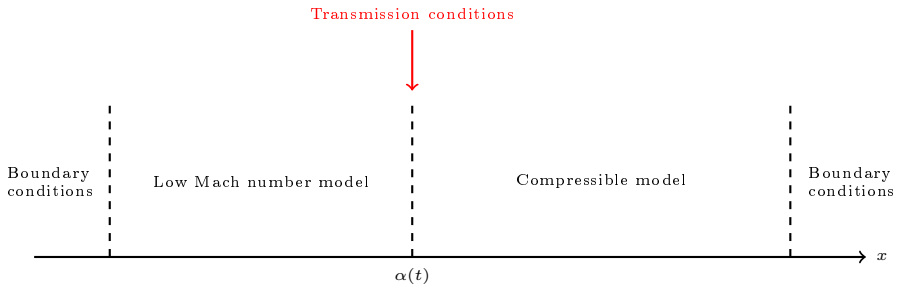

Figure 1: Coupling strategy

depending on characteristic time / length scales of the underlying experiment.

Although the aforementioned new models yield a good balance between physical content and computational performance, they might become unrelevant. Indeed, nothing ensures that the overall system would remain in the regime we are focusing on. The heat release for example might make the velocity field increase so that the local Mach number could not be considered small anymore. Even if the failure of our main assumption is localized in time/space, it has to be taken into account. That is why we investigate in this paper a new pathway in modelling low Mach number flows which incorporates the parent compressible model. Actually, we aim at coupling the compressible Euler equations with its low Mach number approximation through an interface moving according to the order of magnitude of the Mach number (see Figure 1).

Interfaces are inherent in fluid mechanics. We give a brief overview of thin interfaces below.[1] They raise several modelling, mathematical and numerical issues, such as the location of the interfaces, information that can be specified across (transmission conditions), the well-posedness of the coupling problem or the guarantee that the numerical treatment of the transmission conditions would not generate unphysical phenomena. Interface modelling can be split into two main categories:

- *Physical interfaces*: the interface corresponds to a discontinuity surface or to a change of physical properties of the flow. For example, a bubbly flow can be modelled by means of different PDEs for each phase [1]. The interface matches the surface of the bubble. More generally, it occurs in multiphysics problems where fluids have significantly different behaviours within the flow.

  The same model can also be used on each side of the interface but characterized by distinct parameters. For instance, in [9], the interface is prescribed by the discontinuity of the diffusion coefficient of an elliptic equation. It is handled by means of suitable interpolation operators in the framework of a finite-difference method. In [3,19,20], 1D conservation laws are involved with different fluxes: only differs the equation of state between the two domains. Coupling is achieved by an intermediate state approach relying on a Riemann problem at the fixed interface. However models can be completely different when the physics is: pioneering papers concern the coupling between Stokes and Darcy equations for the modelling of porous media [31,36]. Models are coupled by heuristic transmission conditions like the Beavers–Joseph-Saffman condition. Likewise, HEM/HRM coupling is investigated in [2]: in a subdomain, thermodynamic equilibrium is assumed, which legitimates the use of the HEM model. Notice that the HRM model can be seen as a relaxation of the previous one, which dictates the numerical strategy.

- *Fictitious interfaces*: they are concerned with modelling or computational issues. Contrary to the previous type, these interfaces are not motivated by any physical discrepancy. Transmission

[1] Diffuse interfaces are not evoked in this paper.

conditions are thereby mainly based on continuity requirements. For example, domain decomposition methods (the reader could refer to [41]) rely on the creation of arbitrary interfaces. The original domain is split in order to fasten computations through a parallelization procedure. These techniques inspired subsequent works aimed at modelling flows with different regimes. In [17, 18], a steady advection-diffusion equation is studied. The diffusion coefficient is assumed to be small in a part of the domain where the simple advection equation is considered. The strategy consists in optimizing the transmission conditions in the Fourier space.

This kind of interfaces are generally involved in the modelling of complex systems like in the nuclear industry [3]. Several codes corresponding to different loops must be coupled to obtain a solution to the overall problem. Interfaces are then located at the junction of the loops but do not rely on specific physical behaviours. For instance in [24], the coupling between a 1D model (for a pipe) and a 2D one (for the core) is realized.

No matter what the kind of interfaces, two mathematical approaches can be contemplated in proceeding the analysis of the coupling. In the first one, the coupling problem is considered as a whole: if both systems of PDEs can be interpreted as deriving from the same parent model, this latter is solved over the whole domain and specific post-treatments are then carried out in each subdomain to recover the correct behaviour. Interfaces are implicitly included in the formulation. This is in particular the case when one system is a relaxation of the other (like in [2]).

The second approach consists in considering two Initial Boundary Value Problems (IBVP), one for each subdomain. Transmission conditions are used as boundary conditions on both sides of the interface in order to close each IBVP. The issue of well-posedness not only requires the well-posedness of each IBVP individually, but also relies on a suitable handling of transmission conditions. From a numerical point of view, dedicated schemes can be used in each subdomain but the way the two schemes are coupled is a major issue.

In the present work, we investigate the second approach through relevant transmission conditions (see Figure 1). This enables to use specific numerical schemes for each part to make advantage of the properties of each model. We assess the overall numerical strategy by focusing on steady states insofar as they are of great interest in the nuclear industry. Moreover, this enables to yield new explicit solutions to both models which is not possible in the unsteady case. As it will be seen in the core of the paper, naive strategies do not lead to satisfying results due to instabilities and the robustness of algorithms due to the interface is a key point.

The two main contributions of this paper are on the one hand the construction of a steady solution of the coupled problem (Prop. 4) for this choice of interfacial conditions by means of the resolution of a single algebraic equation (4.5); on the other hand, we propose a robust and stable algorithm (§ 5.2) that enables to simulate unsteady solutions of the coupled problem.

The paper is organized as follows: the underlying models are presented in Section 2 as well as their 1D formulations. The coupling strategy is then detailed relying upon the continuity of physical variables. Each model is studied separately in Section 3 in order to provide a better understanding of the limiting process as the Mach number goes to 0. This study includes explicit expressions for steady solutions to both systems of PDEs. These steady states are useful to assess the relevance of the transmission conditions chosen previously, which is achieved in Section 4 where a coupled steady state is constructed. Section 5 then consists of the design of an algorithm for the coupled problem based on two specific numerical schemes in the unsteady case. Some coupling simulations are finally carried out and results are compared to the aforementioned steady states.

2 Models

In the sequel, $\Omega \subset \mathbb{R}^d$, $d \in \{1,2,3\}$, will denote the physical domain which will be divided into two parts depending on the order of magnitude of the Mach number. However, in order to investigate each model independently, we introduce a general bounded domain $\varpi \subset \mathbb{R}^d$.

2.1 Basic equations

To describe the motion of the underlying fluid, we present two models set in ϖ. The first model consists of the standard Euler equations with an energy source term

$$\partial_t \mathbf{W} + \nabla \cdot \mathbf{F}(\mathbf{W}) = \mathbf{\Phi}, \tag{2.1a}$$

with

$$\mathbf{W} = \begin{pmatrix} \rho \\ \rho \boldsymbol{u} \\ \rho E \end{pmatrix}, \qquad \mathbf{F}(\mathbf{W}) = \begin{pmatrix} \rho \boldsymbol{u} \\ \rho \boldsymbol{u} \otimes \boldsymbol{u} + p \mathcal{I}_d \\ (\rho E + p)\boldsymbol{u} \end{pmatrix}, \qquad \mathbf{\Phi} = \begin{pmatrix} 0 \\ 0 \\ \Phi \end{pmatrix}. \tag{2.1b}$$

The source term enables both to enrich the modelling (see below) and to provide nontrivial steady states. The equation of state used to model the fluid properties and to close the system is the ideal fluid law:[2]

$$E = (\Upsilon - 1)\frac{p}{\rho} + \frac{1}{2}|\boldsymbol{u}|^2, \ \Upsilon > 1.$$

The second model is derived from the previous one (2.1) under the hypothesis that the Mach number is "small". Although the Euler equations (2.1) are still valid, they can be simplified by taking into account the order of magnitude of the Mach number. Indeed, some terms become negligible as the Mach number goes to 0. A formal asymptotic expansion (wrt the Mach number) is then carried out in (2.1) similarly to [12,29,33,45]. The resulting system keeping only terms of order 0 is

$$\begin{cases} \partial_t \rho + \nabla \cdot (\rho \boldsymbol{u}) = 0, & \text{(2.2a)} \\ \partial_t (\rho \boldsymbol{u}) + \nabla \cdot (\rho \boldsymbol{u} \otimes \boldsymbol{u}) + \nabla \pi = 0, & \text{(2.2b)} \\ \nabla \cdot \boldsymbol{u} = \dfrac{1}{\Upsilon} \dfrac{\Phi(t,\boldsymbol{x})}{\mathcal{P}(t)} - \dfrac{\Upsilon - 1}{\Upsilon} \dfrac{\mathcal{P}'(t)}{\mathcal{P}(t)}. & \text{(2.2c)} \end{cases}$$

Compared to [29], the right hand side of (2.2c) is more general due to the energy source term.

As classically observed in similar approaches, the asymptotic expansion results in a decoupling of the pressure:

- the *thermodynamic pressure* $\mathcal{P}$ which is involved in the equation of state and corresponds to order 0;
- the *dynamic pressure* π that appears in the momentum equation and corresponds to the second-order term.

This fact also implies a change of nature of the equations which turn elliptic–hyperbolic instead of purely hyperbolic. The main consequence is that acoustic waves are filtered out. Hence remaining waves are travelling at the material velocity.

[2] Instead of the standard Euler constant γ, we introduce $\Upsilon := \frac{\gamma}{\gamma - 1}$ which is more convenient in the present study.

Another remark is that System (2.2) seems to be incomplete as there are more unknowns than equations due to the extra variable π. An additional equation is then required. In this direction, we notice that a direct integration of (2.2c) leads to

$$\frac{\mathcal{P}'(t)}{\mathcal{P}(t)} = \frac{\Upsilon}{(\Upsilon-1)|\varpi|}\left(\frac{1}{\Upsilon\mathcal{P}(t)}\int_{\varpi}\Phi(t,\boldsymbol{x})\,\mathrm{d}\boldsymbol{x} - \int_{\partial\varpi}\boldsymbol{u}\cdot\boldsymbol{n}\,\mathrm{d}\sigma\right). \tag{2.3}$$

This equality provides a relation between the mean pressure and the boundary conditions on the velocity. Two cases must be considered:

- Either pressure $\mathcal{P}$ is known from the underlying experiment and (2.3) provides a constraint upon the boundary velocity (which may induce a coupling strategy);
- Or the velocity is prescribed on the boundary and (2.3) is an ordinary differential equation that enables to compute the pressure.

In the sequel, we shall always consider that one of these cases is matched which provides the required closure equation.

2.2 IBVP in the 1D case

We detail here initial (IC) and boundary conditions (BC). From now on, we focus on dimension 1 with

$$\varpi = (a,b).$$

The two previous models respectively reduce to

$$\begin{cases} \partial_t\rho + \partial_x(\rho u) = 0, & \text{(2.4a)}\\ \partial_t(\rho u) + \partial_x(\rho u^2 + p) = 0, & \text{(2.4b)}\\ \partial_t(\rho E) + \partial_x(\rho E u + p u) = \Phi, & \text{(2.4c)} \end{cases}$$

and to

$$\begin{cases} \partial_t\rho + \partial_x(\rho u) = 0, & \text{(2.5a)}\\ \partial_x u = \dfrac{\Phi(t,x)}{\Upsilon\mathcal{P}(t)} - \dfrac{\Upsilon-1}{\Upsilon}\dfrac{\mathcal{P}'(t)}{\mathcal{P}(t)}, & \text{(2.5b)}\\ \partial_t(\rho u) + \partial_x(\rho u^2 + \pi) = 0. & \text{(2.5c)} \end{cases}$$

In the framework of nuclear modelling, Φ models the heating of the coolant fluid due to fusion reactions in the reactor core. Moreover, we are interested in the following boundary conditions

$$\begin{cases} \rho(t,a) = \varrho_e(t), & \text{(2.6a)}\\ u(t,a) = \mathfrak{u}_e(t), & \text{(2.6b)}\\ p(t,b) = \mathcal{P}_s(t), & \text{(2.6c)} \end{cases}$$

where ϱ_e, $\mathfrak{u}_e$ and $\mathcal{P}_s$ are some positive functions.

As for initial conditions, in accordance with (2.6) we impose

$$\begin{cases} \rho(0,x) = \varrho_0(x), & \text{(2.7a)}\\ u(0,x) = \mathfrak{u}_0(x), & \text{(2.7b)}\\ p(0,x) = p_s, & \text{(2.7c)} \end{cases}$$

where ϱ_0, $\mathfrak{u}_0$ and p_s are some data which are compatible with BC (2.8), *i.e.* such that $\varrho_0(x=a) = \varrho_e(t=0)$, $\mathfrak{u}_0(x=a) = \mathfrak{u}_e(t=0)$ and $p_s = \mathcal{P}_s(0)$. These two models are studied in Section 3.

2.3 The coupled problem

Models like (2.2) have been introduced for two main reasons: first, they are hoped to produce less expensive algorithms; secondly, they enable to tackle the issue of numerical instabilities due to the low Mach number. As the Mach number is commonly assumed to be small in nuclear processes [12,38], it seems natural to make use of System (2.5) in the framework of the present study. However, as accidental events may occur, the Mach number may increase dramatically so that it cannot be assumed to be small anymore.

That is why an adaptive strategy is considered here. We introduce two domains: $\Omega = (0, L)$ models the core of the nuclear reactor (L is thus the length of the core) and $\omega(t) = \big(0, \alpha(t)\big)$ is the subdomain of Ω where the Mach number is small. Here α is a given number such that $0 \leq \alpha \leq L$. The tuning of α will be discussed in the numerical part of this paper (see Section 5).

We are interested in the coupling between the low Mach number model (2.5) set in $\omega(t) = \big(0, \alpha(t)\big)$ and the Euler system (2.4) set in $\Omega \backslash \omega(t) = \big(\alpha(t), L\big)$. BC at the boundary of Ω are

$$\begin{cases} \rho(t,0) = \varrho_e(t), & \text{(2.8a)} \\ u(t,0) = \mathfrak{u}_e(t), & \text{(2.8b)} \\ p(t,L) = p_s. & \text{(2.8c)} \end{cases}$$

The point is to provide transmission conditions on $\partial\omega(t) \cap \Omega = \{\alpha(t)\}$ to connect Systems (2.4) and (2.5). Several strategies may be classically contemplated such as the continuity of physical variables, conservative variables or fluxes.

We propose to couple the two systems through the following continuity conditions

$$\begin{cases} \rho^{(2.5)}\big(t, \alpha^-(t)\big) = \rho^{(2.4)}\big(t, \alpha^+(t)\big), & \text{(2.9a)} \\ u^{(2.5)}\big(t, \alpha^-(t)\big) = u^{(2.4)}\big(t, \alpha^+(t)\big), & \text{(2.9b)} \\ \mathcal{P}^{(2.5)}(t) = p^{(2.4)}\big(t, \alpha^+(t)\big), & \text{(2.9c)} \end{cases}$$

and

$$\pi^{(2.5)}\big(t, \alpha^-(t)\big) = 0. \qquad \text{(2.9d)}$$

The exponent denotes the system to which the variable is a solution. Condition (2.9d) comes from the fact that π is known up to a constant. To fix it, we decided to rely on the asymptotic development where π is the 2nd-order term. The boundary condition is thus supported by the 0th-order term $\mathcal{P}$ through (2.9c). This strategy is depicted on Figure 2.

This choice relies on the particular boundary conditions that are considered in the present study (imposed upon physical variables). Moreover, we emphasize that no physical phenomenon (which may induce discontinuities) is expected to happen at the fictitious interface ($\omega(t)$ is chosen so that no acoustic effect is predominant in its vicinity). The theoretical study of this strategy is presented in Section 4 and numerical applications in Section 5.

3 Unsteady and steady solutions of individual models

From now on, we assume that the source term is constant $\Phi(t,x) \equiv \Phi_0 > 0$. Extensions to $\Phi = \Phi(x)$ are straightforward (see Corollary 3 for example).

Before establishing the coupling strategy, we wish to better understand the properties of each model and especially the influence of the asymptotic expansion on steady states. **We thus do not investigate**

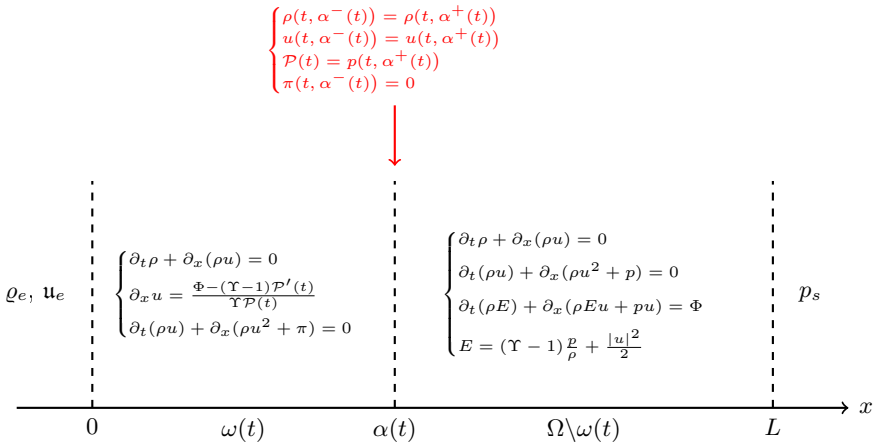

Figure 2: Setting of the coupling problem

the coupling in this section but we study each system independently from each other in $\varpi = (a,b)$ together with BC (2.6).

3.1 Unsteady solutions

The nature of the Euler equations which form a hyperbolic system of PDEs induces numerous difficulties. In particular, boundary conditions are imposed by the sign of characteristic fields which is not known *a priori*. The regularity of solutions is also influenced by hyperbolicity, as discontinuities may form in finite time no matter how smooth the data [8,44]. An extensive literature has been devoted to the well-posedness of Euler equations but some problems are still open. Likewise, few explicit solutions are known except for simple Riemann problems [46]. Hence, few things can be stated about unsteady solutions for the compressible model (2.4).

On the contrary, the mathematical structure of the low Mach number system (2.5) is different from the Euler equations as it is hyperbolic-elliptic. A main consequence in 1D is that we can provide explicit unsteady solutions similarly to [4,5]:

Proposition 1. *System (2.5) together with BC (2.6) and IC (2.7) has a unique solution given by*

$$\begin{cases}
\rho^{\mathrm{LM}}(t,x) = \varrho_e(t^*)\cdot\left[\dfrac{\mathcal{P}_s(t)}{\mathcal{P}_s(t^*)}\right]^{(\Upsilon-1)/\Upsilon}\exp\left[-\dfrac{\Phi_0}{\Upsilon}\big(\Pi_s(t)-\Pi_s(t^*)\big)\right], \\
\qquad\qquad \textit{if there exists } t^*\in(0,t) \textit{ such that } \chi(t^*;t,x)=0, & (3.1a)\\
\rho^{\mathrm{LM}}(t,x) = \varrho_0\big(\chi(0;t,x)\big)\cdot\left[\dfrac{\mathcal{P}_s(t)}{\mathcal{P}_s(0)}\right]^{(\Upsilon-1)/\Upsilon}\exp\left[-\dfrac{\Phi_0}{\Upsilon}\big(\Pi_s(t)-\Pi_s(0)\big)\right], \\
\qquad\qquad \textit{otherwise}, & (3.1b)\\
\mathcal{P}(t) = \mathcal{P}_s(t), & (3.1c)\\
u^{\mathrm{LM}}(t,x) = \mathfrak{u}_e(t) + \left[\dfrac{\Phi_0}{\Upsilon\mathcal{P}_s(t)} - \dfrac{\Upsilon-1}{\Upsilon}\dfrac{\mathcal{P}_s'(t)}{\mathcal{P}_s(t)}\right](x-a). & (3.1d)
\end{cases}$$

Π_s denotes a primitive function of $1/\mathcal{P}_s$ and χ is the characteristic flow given by (3.3).

Proof. On the one hand, we notice that (3.1c) is a direct consequence of BC (2.6c). On the other hand, Eq. (2.5b) can be directly integrated applying BC (2.6b) which yields (3.1d).

The velocity field being known, we can compute the density by applying the method of characteristics to Eq. (2.5a). Let χ be the characteristic flow associated with u^{LM}, *i.e.* solution to the ODE

$$\begin{cases} \dfrac{\mathrm{d}\chi}{\mathrm{d}\tau} = u^{\mathrm{LM}}\big(\tau, \chi(\tau)\big), \\ \chi(t) = x. \end{cases} \tag{3.2}$$

Due to classical smoothness results [10], the solution of this ordinary differential equation (ODE) depends continuously on t and x which are considered as parameters. That is why the solution to (3.2) is denoted by $\chi(\tau; t, x)$ in the sequel (or simply $\chi(\tau)$ if no confusion is possible). Thanks to (3.1d), ODE (3.2) reads

$$\left\{ [\chi(\tau) - a] \exp\left[\frac{-\Phi_0 \Pi_s(\tau) + (\Upsilon - 1)\ln \mathcal{P}_s(\tau)}{\Upsilon} \right] \right\}' = \mathfrak{u}_e(\tau) \exp\left[-\frac{\Phi_0 \Pi_s(\tau) + (\Upsilon - 1)\ln \mathcal{P}_s(\tau)}{\Upsilon} \right].$$

A direct integration leads to

$$\begin{aligned} \chi(\tau; t, x) = a + (x - a) \left[\frac{\mathcal{P}_s(t)}{\mathcal{P}_s(\tau)} \right]^{(\Upsilon-1)/\Upsilon} \exp\left[\frac{\Phi_0}{\Upsilon} \big(\Pi_s(\tau) - \Pi_s(t) \big) \right] \\ + \int_t^\tau \mathfrak{u}_e(\sigma) \left[\frac{\mathcal{P}_s(\sigma)}{\mathcal{P}_s(\tau)} \right]^{(\Upsilon-1)/\Upsilon} \exp\left[\frac{\Phi_0}{\Upsilon} \big(\Pi_s(\tau) - \Pi_s(\sigma) \big) \right] \mathrm{d}\sigma. \end{aligned} \tag{3.3}$$

Setting $\varrho(\tau) = \rho^{\mathrm{LM}}\big(\tau, \chi(\tau; t, x)\big)$ and using the divergence constraint (2.5b), Eq. (2.5a) can be written

$$\varrho'(\tau) = -\varrho(\tau) \partial_x u^{\mathrm{LM}}\big(\tau, \chi(\tau; t, x)\big) = \frac{(\Upsilon - 1)\mathcal{P}_s'(\tau) - \Phi_0}{\Upsilon \mathcal{P}_s(\tau)} \varrho(\tau).$$

Hence:

$$\rho^{\mathrm{LM}}\big(\tau, \chi(\tau; t, x)\big) = \rho(t, x) \cdot \left[\frac{\mathcal{P}_s(\tau)}{\mathcal{P}_s(t)} \right]^{(\Upsilon-1)/\Upsilon} \exp\left[-\frac{\Phi_0}{\Upsilon} \big(\Pi_s(\tau) - \Pi_s(t) \big) \right].$$

Two cases must be considered depending on (t, x):

- either the characteristic curve $\tau \mapsto \chi(\tau; t, x)$ reaches the boundary $x = a$ for some $t^*(t, x) \in (0, t)$, *i.e.* $\chi(t^*; t, x) = 0$ which, due to (2.6a), leads to (3.1a);
- or the characteristic curve lies in ϖ for all $\tau \in (0, t)$. Then, for $\tau = 0$, we obtain (3.1b).

□

Remark 1. *Solution (3.1) is a generalization of [4, Prop. 3.1] for variable output pressure and inlet velocity. Indeed, when $\mathcal{P}_s(t) = p_s$ and $\mathfrak{u}_e(t) = \bar{\mathfrak{u}}_e$, the previous expressions can be made explicit. We have*

$$t^*(t, x) = t - \frac{\Upsilon p_s}{\Phi_0} \ln\left(1 + \frac{\Phi_0}{\Upsilon p_s \bar{\mathfrak{u}}_e} (x - a) \right).$$

Hence

$$\rho^{\mathrm{LM}}(t, x) = \begin{cases} \rho_0\big(\chi(0; t, x)\big) \exp\left[-\frac{\Phi_0 t}{\Upsilon p_s} \right], & \text{if } t < \frac{\Upsilon p_s}{\Phi_0} \ln\left(1 + \frac{\Phi_0}{\Upsilon p_s \bar{\mathfrak{u}}_e} (x - a) \right), \\ \dfrac{\rho_e\big(t^*(t, x)\big)}{1 + \frac{\Phi_0}{\Upsilon p_s \bar{\mathfrak{u}}_e} (x - a)}, & \text{otherwise.} \end{cases}$$

3.2 Steady solutions

As we have no explicit unsteady solutions for the compressible equations, we cannot analyze the influence of the low Mach number assumption. This made us focus on steady states in order to provide a qualitative study. Thus we assume in this section that ϱ_e and $\mathfrak{u}_e$ are some constants and that $\mathcal{P}_s(t) = p_s$.

3.2.1 Compressible model

Contrary to the unsteady case, we are able to derive in this paragraph explicit expressions for steady solutions to System (2.4) supplemented with BC (2.6). The derivation of such solutions for the Euler equations in the transonic case and their physical/numerical stability have been studied for example in [16] (in the case $\Phi = 0$, without energy and with variable area).

$D_e := \varrho_e \mathfrak{u}_e$ denotes the inflow rate. We introduce the following nondimensionalized coefficients

$$\widetilde{p}_s = \frac{p_s \varrho_e}{D_e^2}, \ \widetilde{\Phi} = \frac{2\Phi_0 \varrho_e^2 (b-a)}{D_e^3}. \tag{3.4}$$

In the sequel, $\widetilde{\ }$ will denote variables without dimension. We also recall that $\Upsilon > 1$.

Proposition 2. *Let us assume that the physical and boundary data satisfy the inequality*

$$\widetilde{p}_s > \frac{\Upsilon - 1}{\Upsilon} \left(1 + \sqrt{\frac{\widetilde{\Phi}}{2\Upsilon - 1}} \right). \tag{H1}$$

Then System (2.4) set in (a,b) with boundary conditions (2.6) admits the following steady state

$$\begin{cases} \rho_\infty(x) = \varrho_e \dfrac{\Upsilon(\widetilde{p}_e + 1) + \sqrt{(\Upsilon \widetilde{p}_e - \Upsilon + 1)^2 - (2\Upsilon - 1)\widetilde{\Phi}\frac{x-a}{b-a}}}{2\Upsilon \widetilde{p}_e + 1 + \widetilde{\Phi}\frac{x-a}{b-a}}, \\ p_\infty(x) = \dfrac{D_e^2}{(2\Upsilon - 1)\varrho_e} \left[(\Upsilon - 1)(\widetilde{p}_e + 1) + \sqrt{(\Upsilon \widetilde{p}_e - \Upsilon + 1)^2 - (2\Upsilon - 1)\widetilde{\Phi}\frac{x-a}{b-a}} \right], \\ u_\infty(x) = \dfrac{D_e}{(2\Upsilon - 1)\varrho_e} \left[\Upsilon(\widetilde{p}_e + 1) - \sqrt{(\Upsilon \widetilde{p}_e - \Upsilon + 1)^2 - (2\Upsilon - 1)\widetilde{\Phi}\frac{x-a}{b-a}} \right], \end{cases} \tag{3.5}$$

where $\widetilde{p}_e := (\Upsilon - 1)(1 - \widetilde{p}_s) + \sqrt{(\Upsilon \widetilde{p}_s - \Upsilon + 1)^2 + \widetilde{\Phi}}$.

Notice that $p_\infty(a) = \frac{D_e^2 \widetilde{p}_e}{\varrho_e}$.

Corollary 1. *Hypothesis (H1) corresponds to a subsonic configuration,* i.e. *the Mach number* $\max_x \mathcal{M}_\infty(x)$ *associated with (3.5) is lower than* 1.

Proposition 3. *Let us assume that the data satisfy the inequalities*

$$\widetilde{\Phi} < \frac{(\Upsilon - 1)^2}{2\Upsilon - 1}, \qquad \wp < \widetilde{p}_s < \frac{\Upsilon - 1}{\Upsilon} \left(1 - \sqrt{\frac{\widetilde{\Phi}}{2\Upsilon - 1}} \right), \tag{H2}$$

where $\wp = \frac{\Upsilon-1}{2\Upsilon-1}\left(1-\sqrt{1-\frac{2\Upsilon-1}{(\Upsilon-1)^2}\widetilde{\Phi}}\right)$. *Then System* (2.4) *set in* (a,b) *with boundary conditions* (2.6) *admits the following steady state*

$$\begin{cases} \rho_\infty(x) = \varrho_e \dfrac{\Upsilon(\widetilde{p}_e+1) - \sqrt{(\Upsilon\widetilde{p}_e-\Upsilon+1)^2 - (2\Upsilon-1)\widetilde{\Phi}\frac{x-a}{b-a}}}{2\Upsilon\widetilde{p}_e+1+\widetilde{\Phi}\frac{x-a}{b-a}}, \\ p_\infty(x) = \dfrac{D_e^2}{(2\Upsilon-1)\varrho_e}\left[(\Upsilon-1)(\widetilde{p}_e+1) - \sqrt{(\Upsilon\widetilde{p}_e-\Upsilon+1)^2 - (2\Upsilon-1)\widetilde{\Phi}\frac{x-a}{b-a}}\right], \\ u_\infty(x) = \dfrac{D_e}{(2\Upsilon-1)\varrho_e}\left[\Upsilon(\widetilde{p}_e+1) + \sqrt{(\Upsilon\widetilde{p}_e-\Upsilon+1)^2 - (2\Upsilon-1)\widetilde{\Phi}\frac{x-a}{b-a}}\right], \end{cases} \tag{3.6}$$

where $\widetilde{p}_e := (\Upsilon-1)(1-\widetilde{p}_s) - \sqrt{(\Upsilon\widetilde{p}_s-\Upsilon+1)^2+\widetilde{\Phi}}$.

Corollary 2. *Hypothesis* (H2) *corresponds to a supersonic configuration,* i.e. *the Mach number* $\max_x \mathcal{M}_\infty(x)$ *associated with* (3.6) *is greater than* 1.

Corollary 3. *When* Φ *depends on the space variable (but is still positive), the previous propositions (2 and 3) hold with* $\widetilde{\Phi}$ *and* $\frac{x-a}{b-a}$ *replaced respectively by*

$$\frac{2\varrho_e^2}{D_e^3}\int_a^b \Phi(y)\,\mathrm{d}y \qquad \text{and} \qquad \frac{\int_a^x \Phi(y)\,\mathrm{d}y}{\int_a^b \Phi(y)\,\mathrm{d}y}.$$

Remark 2. *Steady states* (3.5) *and* (3.6) *are not known in the literature to our knowledge. Due to the source term* Φ*, they are not trivial. However, they are smooth functions of* $\widetilde{\Phi}$ *(and thus of* Φ_0*) and when* $\Phi_0 \to 0$*, we recover the standard trivial steady state for the Euler system,* i.e. $(\rho_\infty, u_\infty, p_\infty) = (\varrho_e, \mathfrak{u}_e, p_s)$ *from Prop. 2 for* $\widetilde{p}_s > \frac{\Upsilon-1}{\Upsilon}$ *and from Prop. 3 for* $0 < \widetilde{p}_s < \frac{\Upsilon-1}{\Upsilon}$.

As stated in Prop. 2 and Prop. 3, we cannot always exhibit a steady state. The domain of existence is drawn on Figure 3. Let us make some comments about this graph. The dashed line corresponds to the sonic line. Above this line (dotted area), the flow is subsonic and a steady state can always be computed. The location of boundary conditions is then in accordance with the eigenvalues associated with the Euler system, which are $u-c$, u and $u+c$ where c is the speed of sound. There are two positive eigenvalues (and two input BC) and a negative one (and one output BC).

Below the sonic line, this statement does not hold anymore (3 positive eigenvalues) and we could expect to have no steady state. However, there exists a small domain (dashed area) in the supersonic part. As the trivial state $(\varrho_e, \mathfrak{u}_e, p_s)$ is a stationary solution when $\Phi_0 = 0$ no matter what the regime of compressibility (see Rem. 2), this area looks like a continuous extension in the vicinity of these trivial states.

We make two other remarks about the results of this section. The first one is about uniqueness: as it will be detailed below, the proof goes to show that (3.5) is the unique smooth subsonic steady solution. The second one is that these solutions are some steady solutions but we do not state that they are asymptotic solutions: there is no proof that any unsteady solution would converge as $t \to +\infty$ towards (3.5). Large time behaviour of solutions to Euler equations is indeed an open question which is not treated in this paper.

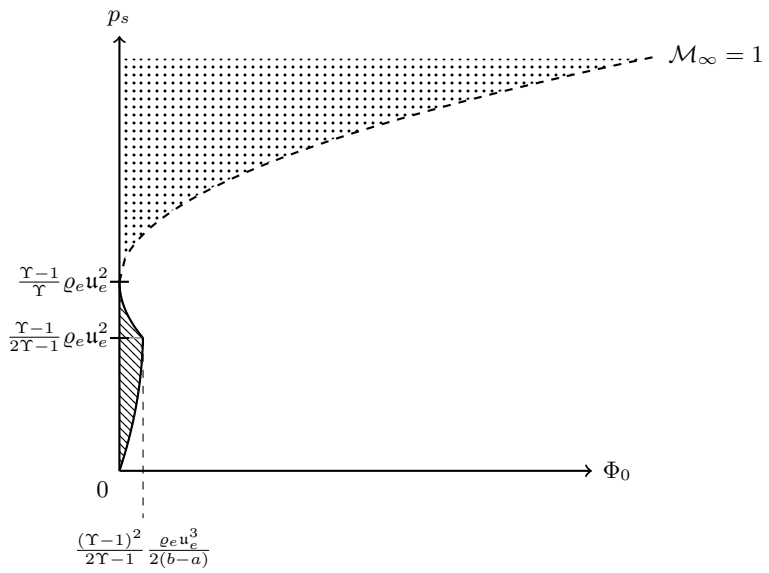

Figure 3: Existence of a steady state in the (Φ_0, p_s) domain: the dotted area corresponds to Prop. 2 ($\mathcal{M}_\infty < 1$) and the hatched domain to Prop. 3 ($\mathcal{M}_\infty > 1$)

Proof of Prop. 2 and 3. We use a shooting method by tuning the inflow pressure $p_e = p_\infty(x = a)$ so that (2.6c) is satisfied. Let us set

$$\widetilde{p}_e = \frac{p_e \varrho_e}{D_e^2}.$$

Integrating (2.4) over (a, x) and taking BC (2.6a-2.6b) into account, the steady states satisfy the equalities

$$\begin{cases} \rho_\infty(x) u_\infty(x) - D_e = 0, & \text{(3.7a)} \\ \rho_\infty(x) u_\infty(x)^2 - \varrho_e \mathfrak{u}_e^2 + p_\infty(x) - p_e = 0, & \text{(3.7b)} \\ \Upsilon p_\infty(x) u_\infty(x) + \frac{1}{2}\rho_\infty(x) u_\infty(x)^3 - \Upsilon p_e \mathfrak{u}_e - \frac{1}{2}\varrho_e \mathfrak{u}_e^3 = \Phi_0(x-a). & \text{(3.7c)} \end{cases}$$

Assuming $\rho_\infty(x) > 0$, Eq. (3.7a) yields

$$u_\infty(x) = \frac{D_e}{\rho_\infty(x)}. \qquad \text{(3.7a')}$$

Due to this relation, (3.7b) reads

$$p_\infty(x) = p_e - D_e^2 \left(\frac{1}{\rho_\infty(x)} - \frac{1}{\varrho_e} \right). \qquad \text{(3.7b')}$$

Inserting relations (3.7a') and (3.7b') into (3.7c) and multiplying by ρ_∞^2, we obtain the following quadratic equation for ρ_∞

$$\rho_\infty(x)^2 \left(\widetilde{\Phi} \frac{x-a}{b-a} + 1 + 2\Upsilon \widetilde{p}_e \right) - 2\Upsilon \varrho_e (1 + \widetilde{p}_e) \rho_\infty(x) + \varrho_e^2 (2\Upsilon - 1) = 0.$$

Then, provided that

$$(2\Upsilon - 1)\widetilde{\Phi} \leq (\Upsilon \widetilde{p}_e - \Upsilon + 1)^2, \qquad \text{(3.8)}$$

the solution is real-valued and reads

$$\rho_\infty(x) = \varrho_e \, \frac{\Upsilon(\widetilde{p}_e + 1) \pm \sqrt{(\Upsilon\widetilde{p}_e - \Upsilon + 1)^2 - (2\Upsilon - 1)\widetilde{\Phi}\frac{x-a}{b-a}}}{2\Upsilon\widetilde{p}_e + 1 + \widetilde{\Phi}\frac{x-a}{b-a}}.$$

The $\pm$-sign is determined by the boundary condition $\rho_\infty(a) = \varrho_e$. Indeed:

$$\rho_\infty(a) = \varrho_e \, \frac{\Upsilon(\widetilde{p}_e + 1) \pm |\Upsilon\widetilde{p}_e - \Upsilon + 1|}{2\Upsilon\widetilde{p}_e + 1}.$$

The requirement $\rho_\infty(a) = \varrho_e$ is thus satisfied depending on the sign of $\Upsilon\widetilde{p}_e - \Upsilon + 1$. More precisely, we have

$$\rho_\infty(x) = \begin{cases} \varrho_e \, \dfrac{\Upsilon(\widetilde{p}_e + 1) + \sqrt{(\Upsilon\widetilde{p}_e - \Upsilon + 1)^2 - (2\Upsilon - 1)\widetilde{\Phi}\frac{x-a}{b-a}}}{2\Upsilon\widetilde{p}_e + 1 + \widetilde{\Phi}\frac{x-a}{b-a}}, & \text{if } \widetilde{p}_e \geq \frac{\Upsilon-1}{\Upsilon}, \\ \varrho_e \, \dfrac{\Upsilon(\widetilde{p}_e + 1) - \sqrt{(\Upsilon\widetilde{p}_e - \Upsilon + 1)^2 - (2\Upsilon - 1)\widetilde{\Phi}\frac{x-a}{b-a}}}{2\Upsilon\widetilde{p}_e + 1 + \widetilde{\Phi}\frac{x-a}{b-a}}, & \text{otherwise.} \end{cases} \tag{3.9a}$$

Consequently (see Appendix A.1), inserting (3.9a) into (3.7b')

$$p_\infty(x) = \begin{cases} \dfrac{D_e^2}{(2\Upsilon - 1)\varrho_e}\left[(\Upsilon - 1)(\widetilde{p}_e + 1) + \sqrt{(\Upsilon\widetilde{p}_e - \Upsilon + 1)^2 - (2\Upsilon - 1)\widetilde{\Phi}\frac{x-a}{b-a}}\right], & \text{if } \widetilde{p}_e \geq \frac{\Upsilon-1}{\Upsilon}, \\ \dfrac{D_e^2}{(2\Upsilon - 1)\varrho_e}\left[(\Upsilon - 1)(\widetilde{p}_e + 1) - \sqrt{(\Upsilon\widetilde{p}_e - \Upsilon + 1)^2 - (2\Upsilon - 1)\widetilde{\Phi}\frac{x-a}{b-a}}\right], & \text{otherwise.} \end{cases} \tag{3.9b}$$

The shooting method then consists in choosing pressure p_e such that $p_\infty(b) = p_s$ in order to match BC (2.6c). To do so, we notice that

$$p_\infty(b) = p_s \overset{(3.9b)}{\iff} (2\Upsilon - 1)\widetilde{p}_s - (\Upsilon - 1)(\widetilde{p}_e + 1) = \pm\sqrt{(\Upsilon\widetilde{p}_e - \Upsilon + 1)^2 - (2\Upsilon - 1)\widetilde{\Phi}}.$$

Squaring both sides of the latter equality shows that $\widetilde{p}_e$ is necessarily a solution to the equation

$$\widetilde{p}_e^2 + 2(\Upsilon - 1)(\widetilde{p}_s - 1)\widetilde{p}_e - (2\Upsilon - 1)\widetilde{p}_s^2 + 2(\Upsilon - 1)\widetilde{p}_s - \widetilde{\Phi} = 0. \tag{3.10}$$

Then

$$\widetilde{p}_e^{\pm} = (\Upsilon - 1)(1 - \widetilde{p}_s) \pm \sqrt{(\Upsilon\widetilde{p}_s - \Upsilon + 1)^2 + \widetilde{\Phi}}. \tag{3.11}$$

We can verify that

$$\pm\left[\widetilde{p}_e^{\pm} - \frac{\Upsilon - 1}{\Upsilon}\right] \geq 0, \tag{3.12a}$$

$$(\Upsilon\widetilde{p}_e^{\pm} - \Upsilon + 1)^2 \geq (2\Upsilon - 1)\widetilde{\Phi}. \tag{3.12b}$$

In fact, on the one hand, (3.12a) is equivalent to $\pm\Lambda_\pm(\mathcal{X}_s) \geq 0$ where

$$\Lambda_\pm(Y) := Y \pm \frac{\Upsilon}{\Upsilon - 1}\sqrt{Y^2 + \widetilde{\Phi}} \qquad \text{and} \qquad \mathcal{X}_s = \Upsilon - \Upsilon\widetilde{p}_s - 1.$$

We easily check that $\Lambda_\pm$ has indeed the sign of $\pm$ over $\mathbb{R}$. On the other hand, (3.12b) comes from the equality (see Appendix A.2)

$$(\Upsilon\widetilde{p}_e^{\pm} - \Upsilon + 1)^2 - (2\Upsilon - 1)\widetilde{\Phi} = \left[\Upsilon\mathcal{X}_s \pm (\Upsilon - 1)\sqrt{\mathcal{X}_s^2 + \widetilde{\Phi}}\right]^2. \tag{3.13}$$

Hence (3.12a) determines the solution in (3.9) through the selection of the relevant case (first case: $\widetilde{p}_e = \widetilde{p}_e^+$; second case: $\widetilde{p}_e = \widetilde{p}_e^-$) while (3.12b) ensures that Hyp. (3.8) holds.

Conversely, let us verify that Solution (3.9) together with $\widetilde{p}_e^\pm$ given by (3.11) is indeed a physically admissible solution to System (2.4) with BC (2.6). First, we check the positivity of $\rho_\infty^\pm$. It is obvious for ρ_∞^+ as the sum of positive terms due to (3.12a) which implies that $\widetilde{p}_e^+ > \frac{\Upsilon-1}{\Upsilon} > 0$. For ρ_∞^-, the numerator is minimal at $x = a$ and the positivity is also a consequence of (3.12a).

We then ensure that $p_\infty^\pm(x = b) = p_s$. We deduce from (3.9b) for $x = b$, from (3.11) and (3.13)

$$p_\infty^\pm(b) = \frac{(\Upsilon-1)D_e^2}{(2\Upsilon-1)\varrho_e}\left((\Upsilon-1)(1-\widetilde{p}_s) + 1 \pm \sqrt{\mathcal{X}_s^2 + \widetilde{\Phi}} \pm \left|\frac{\Upsilon}{\Upsilon-1}\mathcal{X}_s \pm \sqrt{\mathcal{X}_s^2 + \widetilde{\Phi}}\right|\right).$$

We remark that

- $p_\infty^+(b) = p_s$ if and only if

$$\frac{\Upsilon}{\Upsilon-1}\mathcal{X}_s < -\sqrt{\mathcal{X}_s^2 + \widetilde{\Phi}} \iff \mathcal{X}_s < -(\Upsilon-1)\sqrt{\frac{\widetilde{\Phi}}{2\Upsilon-1}} \iff \text{(H1)}. \tag{3.14}$$

  As p_∞^+ is monotone decreasing, we observe that $p_\infty^+(x) \geq p_s > 0$ for all x which ends the proof of Prop. 2 as (3.5) is indeed a physical solution.

- $p_\infty^-(b) = p_s$ if and only if

$$\begin{aligned}\frac{\Upsilon}{\Upsilon-1}\mathcal{X}_s > \sqrt{\mathcal{X}_s^2 + \widetilde{\Phi}} &\iff \mathcal{X}_s > (\Upsilon-1)\sqrt{\frac{\widetilde{\Phi}}{2\Upsilon-1}} \\ &\iff \widetilde{p}_s < \widetilde{p}_* := \frac{\Upsilon-1}{\Upsilon}\left(1 - \sqrt{\frac{\widetilde{\Phi}}{2\Upsilon-1}}\right).\end{aligned} \tag{3.15}$$

  Hence the right part of (H2). Notice that the positivity of $\widetilde{p}_s$ implies that we have

$$\widetilde{\Phi} < 2\Upsilon - 1.$$

  As p_∞^- is monotone-increasing with respect to x, we must then take care of the positivity of $p_e^- = p_\infty^-(a)$ – or equivalently of $\widetilde{p}_e^-$ – in order to ensure that p_∞^- remains positive over (a, b). $\widetilde{p}_e^-$ defined by (3.11) increases as a function of $\widetilde{p}_s$ then decreases. Indeed, as

$$\begin{aligned}(\widetilde{p}_e^-)'(\widetilde{p}_s) &= -(\Upsilon-1) - \Upsilon\frac{\Upsilon\widetilde{p}_s - \Upsilon + 1}{\sqrt{(\Upsilon\widetilde{p}_s - \Upsilon + 1)^2 + \widetilde{\Phi}}}, \\ (\widetilde{p}_e^-)''(\widetilde{p}_s) &= -\frac{\Upsilon^2\widetilde{\Phi}}{\left[(\Upsilon\widetilde{p}_s - \Upsilon + 1)^2 + \widetilde{\Phi}\right]^{3/2}} < 0,\end{aligned}$$

  we induce that $(\widetilde{p}_e^-)'$ is monotone-decreasing and we verify that $(\widetilde{p}_e^-)'(\widetilde{p}_*) = 0$ with $\widetilde{p}_*$ defined by (3.15). Function $\widetilde{p}_e^-$ thus admits a maximum at $\widetilde{p}_*$. The corresponding maximal value

$$\widetilde{p}_e^-(\widetilde{p}_*) = \frac{\Upsilon-1}{\Upsilon} - \frac{2\Upsilon-1}{\Upsilon}\sqrt{\frac{\widetilde{\Phi}}{2\Upsilon-1}}$$

  is positive if and only if $\widetilde{\Phi} < \frac{(\Upsilon-1)^2}{2\Upsilon-1} < 2\Upsilon - 1$. Under that condition, the domain of positivity of $\widetilde{p}_e^-$ wrt $\widetilde{p}_s$ reads $[\wp, \overline{\wp}]$ – see Fig. 4 – where $\wp$, $\overline{\wp}$ are solutions to $\widetilde{p}_e(X) = 0 \iff (2\Upsilon-1)X^2 - 2(\Upsilon-1)X + \widetilde{\Phi} = 0$. Given that $\wp < \widetilde{p}_* < \overline{\wp}$ and $\widetilde{p}_s < \widetilde{p}_*$ according to (3.15), we deduce that (3.6) is a physically admissible solution for $\widetilde{p}_s \in (\wp, \widetilde{p}_*)$.

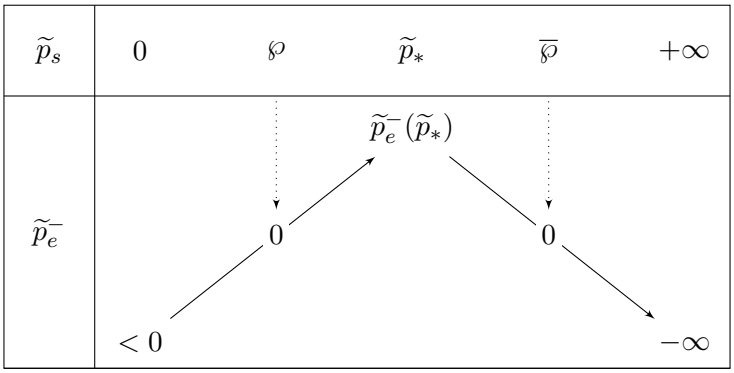

Figure 4: Variations of $\widetilde{p}_e^-(\widetilde{p}_s) = (\Upsilon - 1)(1 - \widetilde{p}_s) - \sqrt{(\Upsilon\widetilde{p}_s - \Upsilon + 1)^2 + \widetilde{\Phi}}$

□

Proof of Corollary 1, page 10 and Corollary 2, page 11. Under the hypotheses of Proposition 2, the local Mach number is given by

$$\mathcal{M}_\infty(x) = \frac{u_\infty(x)}{\sqrt{\frac{\Upsilon p_\infty(x)}{(\Upsilon-1)\rho_\infty(x)}}} = \left(\frac{\Upsilon-1}{\Upsilon}\right)^{1/2} \frac{D_e}{\sqrt{p_\infty(x)\rho_\infty(x)}}$$
$$\overset{(3.7b')}{=} \left(\frac{\Upsilon-1}{\Upsilon}\right)^{1/2} \left[\frac{\rho_\infty(x)}{\varrho_e}(1+\widetilde{p}_e^+) - 1\right]^{-1/2}.$$

As ρ_∞ from (3.5) decreases (see Appendix A.1), we deduce that $\mathcal{M}_\infty$ is monotone-increasing with respect to x and is thus maximal at $x = b$. Moreover

$$\mathcal{M}_\infty(b) = \sqrt{\frac{(\Upsilon-1)D_e u_\infty(b)}{\Upsilon p_s}}$$
$$\overset{(3.5)}{=} \left(\frac{\Upsilon-1}{\Upsilon(2\Upsilon-1)\widetilde{p}_s}\right)^{1/2} \sqrt{\Upsilon(\widetilde{p}_e^+ + 1) - \sqrt{(\Upsilon\widetilde{p}_e^+ - \Upsilon + 1)^2 - (2\Upsilon-1)\widetilde{\Phi}}}. \quad (3.16)$$

We deduce from $(3.11)^+$ and (3.13) that the square root above in (3.16) is equal to

$$\sqrt{(\Upsilon-1)(\mathcal{X}_s+1) + \Upsilon + \Upsilon\sqrt{\mathcal{X}_s^2+\widetilde{\Phi}} - \left|\Upsilon\mathcal{X}_s + (\Upsilon-1)\sqrt{\mathcal{X}_s^2+\widetilde{\Phi}}\right|}$$
$$\overset{(3.14)}{=} \sqrt{(2\Upsilon-1)\left[\mathcal{X}_s + 1 + \sqrt{\mathcal{X}_s^2+\widetilde{\Phi}}\right]}$$

We recall that we set $\mathcal{X}_s = \Upsilon - 1 - \Upsilon\widetilde{p}_s < 0$. Using again (3.14) through $\sqrt{\mathcal{X}_s^2+\widetilde{\Phi}} < -\frac{\Upsilon}{\Upsilon-1}\mathcal{X}_s$, we obtain from (3.16)

$$\mathcal{M}_\infty(x) \le \mathcal{M}_\infty(b) < \left(\frac{\Upsilon-1}{\Upsilon\widetilde{p}_s}\right)^{1/2} \sqrt{1 - \frac{\mathcal{X}_s}{\Upsilon-1}} = \left(\frac{\Upsilon-1}{\Upsilon\widetilde{p}_s}\right)^{1/2} \sqrt{1 - \frac{\Upsilon - \Upsilon\widetilde{p}_s - 1}{\Upsilon-1}} = 1.$$

As for the second case (Prop. 3), the same calculations hold except that $\mathcal{M}_\infty$ is monotone-decreasing and is thus minimal at $x = b$. Under (H2), we obtain similarly $\mathcal{M}_\infty(x) \ge \mathcal{M}_\infty(b) > 1$. □

3.2.2 Low Mach number model

Similarly to Section 3.1, explicit expressions for steady solutions to the low Mach number model (2.5) can be easily derived. This results from direct integrations of the equations.

Lemma 1. *The steady solution associated with System (2.5) reads, according to Notations (3.4)*

$$\begin{cases} \rho_\infty^{\mathrm{LM}}(x) = \dfrac{\varrho_e}{1+\frac{\Phi_0}{\Upsilon p_s \mathfrak{u}_e}(x-a)} = \dfrac{\varrho_e}{1+\frac{1}{2}\frac{\widetilde{\Phi}}{\Upsilon \widetilde{p}_s}\frac{x-a}{b-a}}, \\ p_\infty^{\mathrm{LM}}(x) = p_s, \\ \pi_\infty^{\mathrm{LM}}(x) = \varrho_e \mathfrak{u}_e \frac{\Phi_0}{\Upsilon p_s}(b-x) = \frac{\varrho_e \mathfrak{u}_e^2}{2}\frac{\widetilde{\Phi}}{\Upsilon \widetilde{p}_s}\frac{b-x}{b-a}, \\ u_\infty^{\mathrm{LM}}(x) = \mathfrak{u}_e\left(1+\frac{\Phi_0}{\Upsilon p_s \mathfrak{u}_e}(x-a)\right) = \mathfrak{u}_e\left(1+\frac{1}{2}\frac{\widetilde{\Phi}}{\Upsilon \widetilde{p}_s}\frac{x-a}{b-a}\right). \end{cases} \tag{3.17}$$

Remark 3. *This result easily extends to the case $\Phi = \Phi(x)$ similarly to Corollary 3 by taking $\widetilde{\Phi} = \frac{2\varrho_e^2}{D_e^3}\int_a^b \Phi(y)\,\mathrm{d}y$ and by replacing $\frac{x-a}{b-a}$ by*

$$\frac{\int_a^x \Phi(y)\,\mathrm{d}y}{\int_a^b \Phi(y)\,\mathrm{d}y}.$$

Remark 4. *Unlike the compressible case, the low Mach number model has no restriction: it always admits a steady state and has a mathematical meaning no matter what the underlying Mach regime. If the Mach number increases, the model is still well-posed but looses its physical legitimacy (see Figures 6 and 7). As an example, we notice that $\partial_x u_\infty^{\mathrm{BM}} > 0$ for any $\Phi_0 > 0$ while the sign of $\partial_x u_\infty$ depends of the regime of compressibility: it is positive in the subsonic case (Prop. 2) and negative in the supersonic case (Prop. 3).*

Remark 5. *It is straightforward that the unsteady solution given in Remark 1 converges to the steady one specified in Lemma 1 when $\rho_e(t) \xrightarrow[t\to+\infty]{} \bar{\rho}_e$.*

3.2.3 Link between the two regimes

It is now possible to understand the balance between the different terms in System (2.4) in the zero Mach limit. It will be useful to design actual low Mach situations by means of relevant values for parameters Φ_0 and p_s.

To do so, we formally work out the limit in (3.5) from Prop. 2 as the Mach number goes to 0.[3] The asymptotic low Mach number assumption consists in stating that

$$\forall\, x \in (a,b),\ u_\infty(x)^2 = o\left(\frac{p_\infty(x)}{\rho_\infty(x)}\right). \tag{3.18}$$

In particular, we deduce from (3.18) at $x = a$ and $x = b$

$$\mathfrak{u}_e^2 = o\left(\frac{p_e}{\varrho_e}\right) \quad \text{and} \quad u_\infty(b)^2 = o\left(\frac{p_s}{\rho_\infty(b)}\right),$$

(we recall that $p_e := p_\infty(a)$) or equivalently

$$\frac{1}{\widetilde{p}_e} = o(1) \quad \text{and} \quad \frac{\varrho_e}{\rho_\infty(b)\widetilde{p}_s} = o(1). \tag{3.19a}$$

[3] Solution (3.6) is not concerned as it corresponds to a supersonic configuration.

Given (3.7b') for $x = b$, we have

$$\widetilde{p}_s + \frac{\varrho_e}{\rho_\infty(b)} = \widetilde{p}_e + 1 \quad \Longleftrightarrow \quad 1 + \frac{\varrho_e}{\rho_\infty(b)\widetilde{p}_s} = \frac{\widetilde{p}_e}{\widetilde{p}_s}\left(1 + \frac{1}{\widetilde{p}_e}\right).$$

The asymptotics (3.19a) provide

$$\frac{\widetilde{p}_e - \widetilde{p}_s}{\widetilde{p}_s} = o(1) \quad \Longleftrightarrow \quad \widetilde{p}_e \sim \widetilde{p}_s. \tag{3.19b}$$

Given the expression of $\widetilde{p}_e$, this reads

$$\frac{\Upsilon - 1}{\widetilde{p}_s} - \Upsilon + \sqrt{\left(\frac{\Upsilon - 1}{\widetilde{p}_s} - \Upsilon\right)^2 + \frac{\widetilde{\Phi}}{\widetilde{p}_s^2}} = o(1).$$

From (3.19a) and (3.19b), we deduce that $1/\widetilde{p}_s = o(1)$. Then, due to $\Upsilon = \mathcal{O}(1)$, the latter relation yields

$$-\Upsilon + \sqrt{\Upsilon^2 + \frac{\widetilde{\Phi}}{\widetilde{p}_s^2}} = o(1) \quad \Longrightarrow \quad \widetilde{\Phi} = o(\widetilde{p}_s^2). \tag{3.19c}$$

Asymptotics (3.19) is in accordance with Hyp. (H1). Inserting (3.19) into (3.5), we prove that ρ_∞ from Prop. 2 converges to $\rho_\infty^{\mathrm{LM}}$ from Lemma 1 as the Mach number goes to 0. The convergence of p_∞ and u_∞ follows.

In conclusion, we have:

Lemma 2. *A low Mach number configuration corresponds to the case where*

$$p_s \gg \varrho_e \mathfrak{u}_e^2 \qquad \textit{and} \qquad \Phi_0 \ll \frac{p_s^2}{(b-a)\varrho_e \mathfrak{u}_e}.$$

We then perform some comparisons between steady states for the two models. We take standard values for pressurized water reactors (PWR): $a = 0\,\mathrm{m}$, $b = 4.2\,\mathrm{m}$, $\Upsilon = 1.74$, $\varrho_e = 735\,\mathrm{kg}\cdot\mathrm{m}^{-3}$ and $\mathfrak{u}_e = 5\,\mathrm{m}\cdot\mathrm{s}^{-1}$. For each case, we represent the profile of the power density, the Mach number associated with the compressible steady solution and the comparisons between low Mach/compressible steady densities and velocities.

Case 1. For standard values of the exit pressure and the power density (estimates from Lemma 2 are satisfied), we note on Figure 15 that both solutions match as the Mach number is about $5\cdot 10^{-2}$. In this standard configuration, the low Mach number model turns out to provide a good asymptotic.

Case 2. When the pressure is divided by 100 as in the case of a depressurization incident, the Mach number can no longer be considered small (see Figure 6) and a significant discrepancy appears. In particular, the velocity field is largely overestimated by the low Mach number model.

Case 3. We show on Figure 7 the case of a more sophisticated profile for Φ with two different orders of magnitude within the core (for instance when control rods are in an intermediate position). The Mach number is of order 1 in the highest part of the reactor which induces different behaviours for steady states: in the highest part for the velocity and in the lowest part (although the Mach number is small) for the density. This can be accounted for by the global effect of the elliptic divergence constraint (2.5b) and by the hyperbolic effect of the Euler system (2.4) (upwinding information due to the negative eigenvalue).

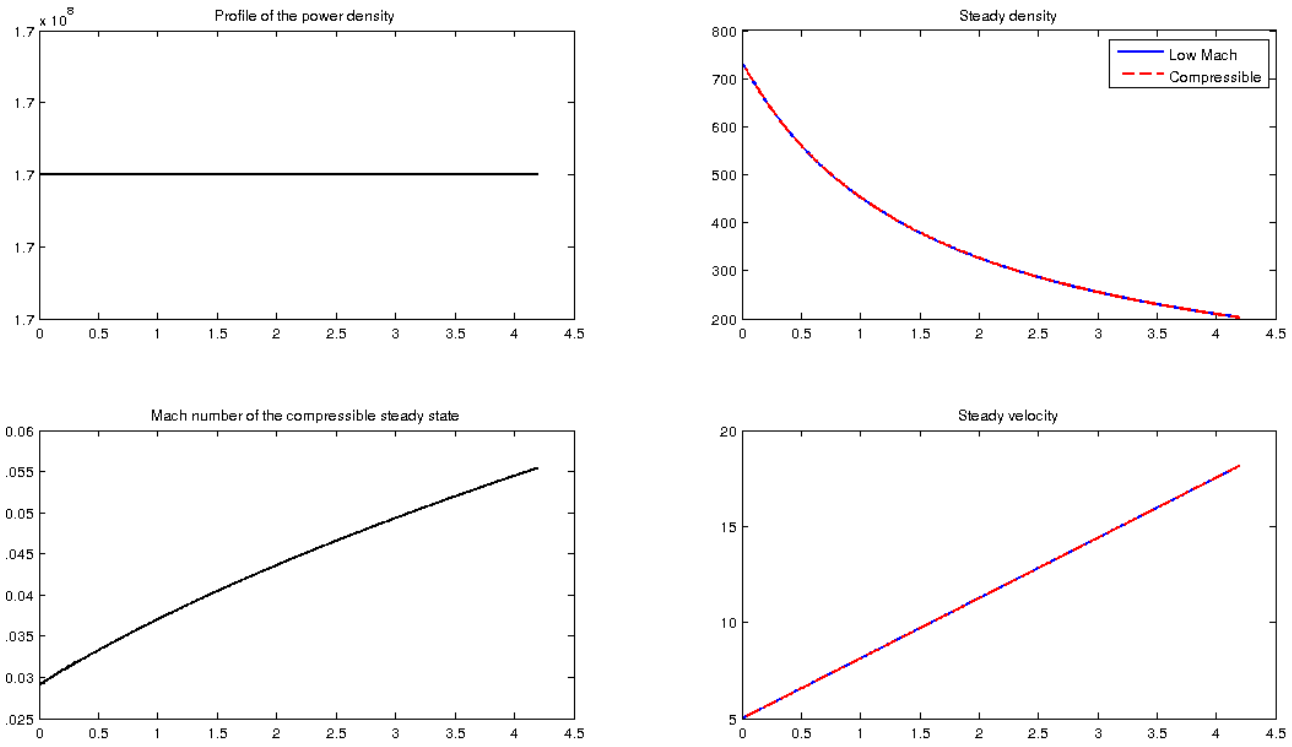

Figure 5: Case 1. $\Phi_0 = 170 \cdot 10^6\,\mathrm{W}\cdot\mathrm{m}^{-3}$, $p_s = 155 \cdot 10^5\,\mathrm{Pa}$

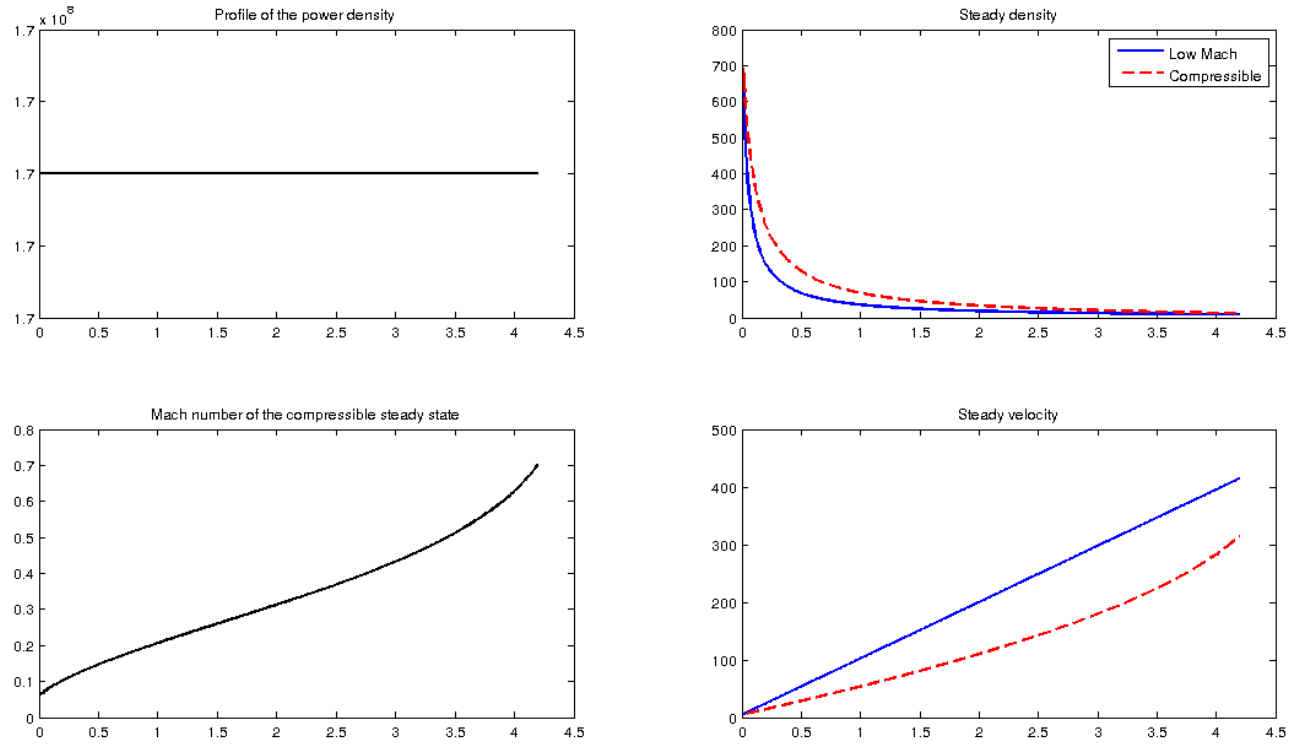

Figure 6: Case 2. $\Phi_0 = 170 \cdot 10^6\,\mathrm{W}\cdot\mathrm{m}^{-3}$, $p_s = 155 \cdot 10^3\,\mathrm{Pa}$

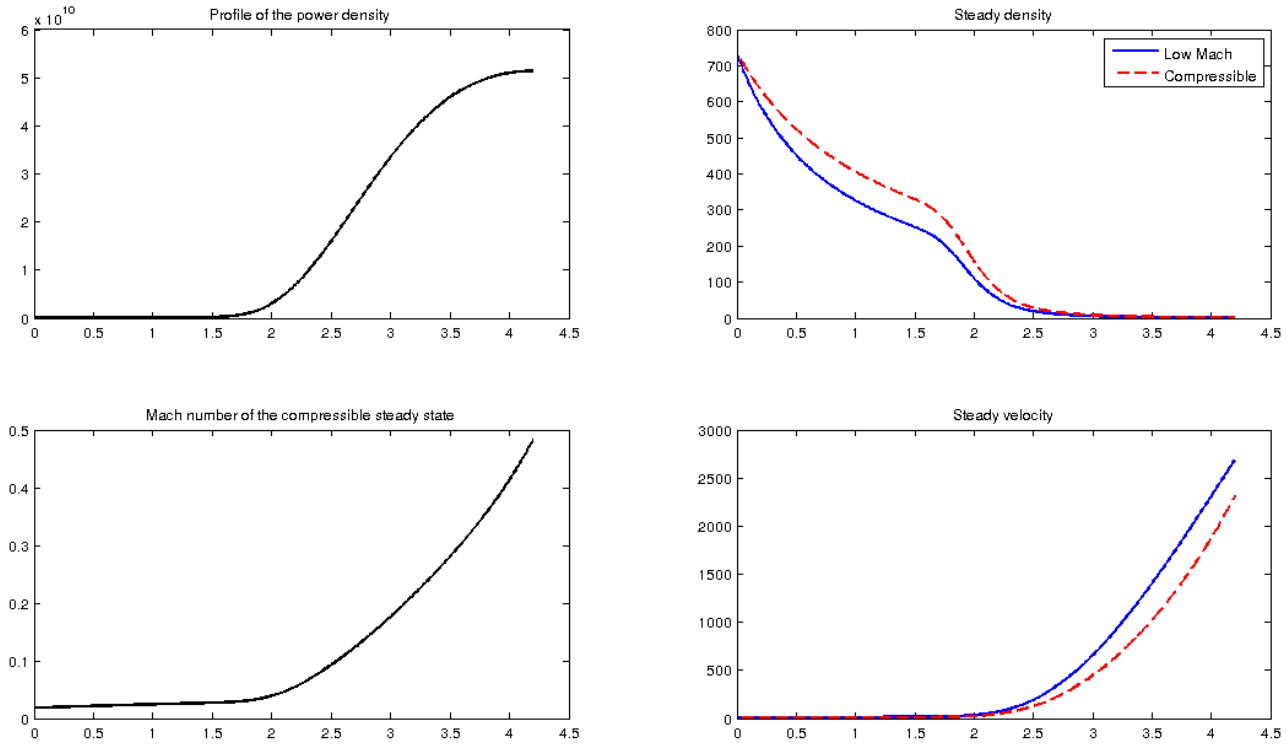

Figure 7: Case 3. $\Phi(x) = \Phi_0 \left[1 + \frac{C_1}{x^3} \exp\left(\frac{-C_2}{x^2}\right)\right]$, $\Phi_0 = 170 \cdot 10^6\,\mathrm{W} \cdot \mathrm{m}^{-3}$, $p_s = 155 \cdot 10^5\,\mathrm{Pa}$

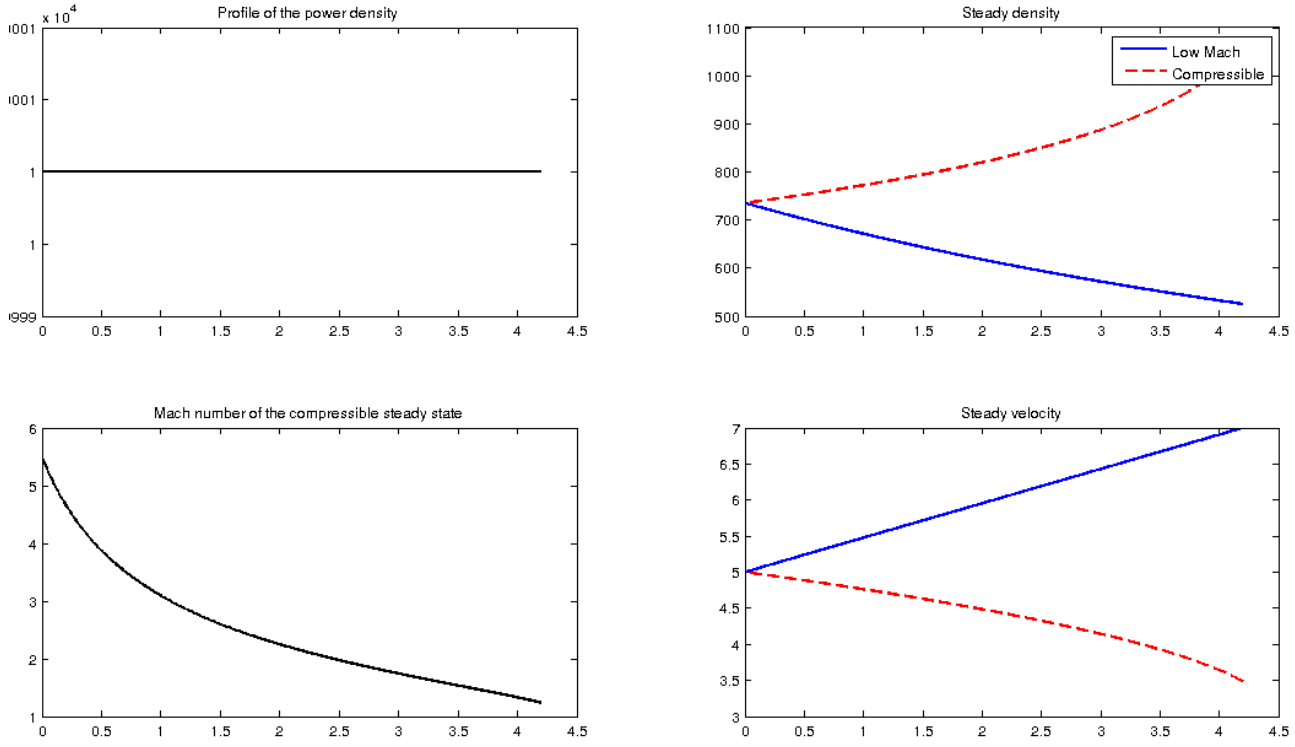

Figure 8: Case 4. $\Phi_0 = 10^4\,\mathrm{W} \cdot \mathrm{m}^{-3}$, $p_s = 6 \cdot 10^3\,\mathrm{Pa}$

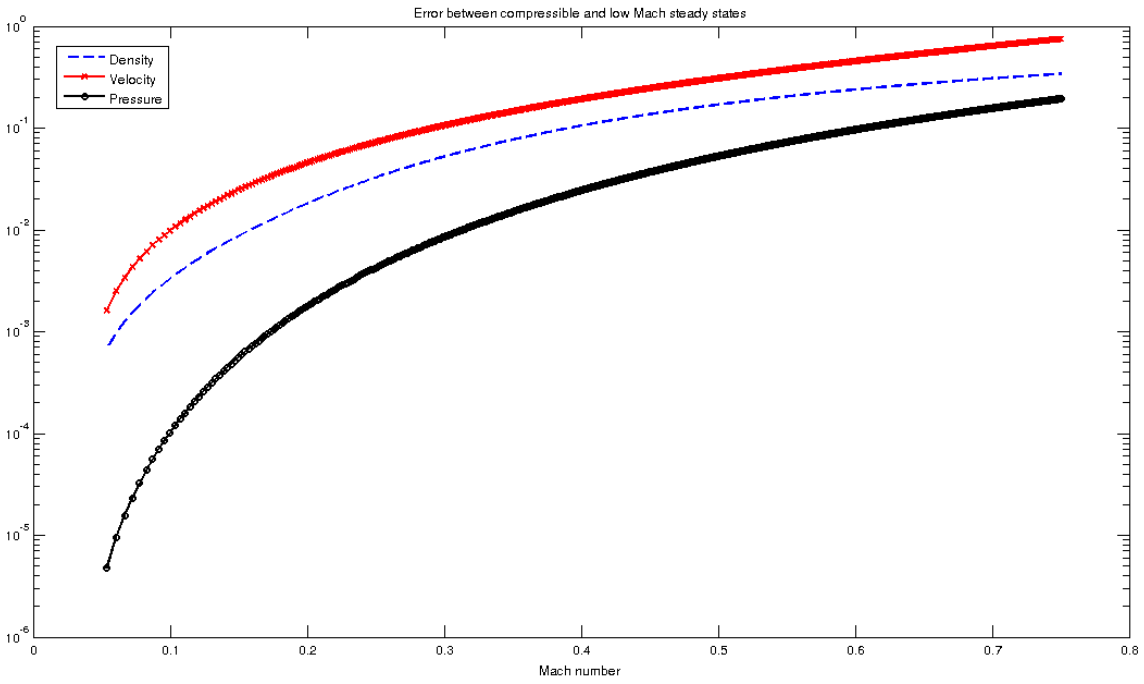

Figure 9: Influence of the Mach number upon the approximation error $\frac{\|\star_\infty^{\mathrm{LM}} - \star_\infty\|}{\|\star_\infty\|}$

Case 4. We present on Figure 8 a supersonic configuration suited to Prop. 3 with smaller values of p_s and Φ_0. We notice different monotonicities of solutions and the low Mach number state is clearly not relevant in this case.

We emphasize on Figure 9 the correlation between the Mach number and the quality of the approximation of the compressible model by the low Mach one. To do so, we take standard values as previously and $p_s = 155 \cdot 10^5$ Pa. To make the Mach number vary, we take Φ_0 in the range $[10^6, 10^9]\,\mathrm{W} \cdot \mathrm{m}^{-3}$. We remark on the figure that errors have the same behaviour whatever the underlying variable. Roughly, for Mach numbers under 0.1, all errors are lower than 10^{-2}.

4 Steady solutions of the coupled problem

This section is devoted to the analysis of the coupling (2.4-2.5) through the transmission conditions (2.9). From now on, we assume that α is a constant lying in $(0, L)$.

For the sake of clarity, we introduce two more notations:

- Given the conservative state $\mathbf{W}$, the pressure is computed through the relation $p = \Pi(\mathbf{W})$.
- Conversely, if the physical variables (ρ, u, p) are known, the conservative is recovered by $\mathbf{W} = \mathcal{W}(\rho, u, p)$.

A naive strategy to construct an unsteady solution to the coupling problem consists in applying an iterative algorithm through the interface (see Figure 2): we first notice that the solution (3.1) of the low Mach number model (2.5) can be parametrized by $\mathcal{P}$. Given $\mathcal{P}^k(t)$, this solution for $x = \alpha$ is injected in (2.9a) and (2.9b) which form the boundary conditions for the compressible model (2.4) over

(α, L) together with (2.8c). In a subsonic framework, the Cauchy problem in the compressible domain admits a solution over some time interval. This solution also depends on $\mathcal{P}^k(t)$ and is denoted by $\mathbf{W}\big(t, x; \mathcal{P}^k(t)\big)$. Then the resulting compressible pressure can be used to update the low Mach pressure $\mathcal{P}^{k+1}(t)$ through the boundary condition (2.9c).

The iterative procedure thus comes down to solving the fixed-point equation

$$\mathcal{P}(t) = \Pi\left(\mathbf{W}\big(t, \alpha^+; \mathcal{P}(t)\big)\right), \tag{4.1}$$

which corresponds to the transmission condition (2.9c). Nevertheless, as the unsteady compressible Euler equations cannot be explicitly solved in this case, the fixed-point problem (4.1) cannot be made explicit. We cannot thus state about the well-posedness of the coupling.

To go further, we get interested in steady states associated with the coupling (2.4-2.5) by using results from Section 3.2. More precisely, we intend to couple:

- solutions from Lemma 1 for $(a, b) = (0, \alpha)$ and some interfacial pressure p_α imposed at $x = \alpha^-$;
- and solutions from Prop. 2 for $(a, b) = (\alpha, L)$ and some interfacial density and velocity ϱ_α and $\mathfrak{u}_\alpha$ imposed at $x = \alpha^+$.

As it will be detailed in the sequel, this procedure comes down to determining the sole parameter p_α ($\varrho_\alpha = \rho_\infty^{\mathrm{LM}}(\alpha)$ and $\mathfrak{u}_\alpha = u_\infty^{\mathrm{LM}}(\alpha)$ depend explicitly on p_α).

We first focus on assumptions on global parameters p_s, Φ_0, ϱ_e and $\mathfrak{u}_e$ so that such a steady state might exist and then we specify the computation of the interfacial pressure which guarantees that the transmission conditions (2.9) are satisfied.

In accordance with previous notations, we set

$$\widetilde{p}_s = \frac{p_s \varrho_e}{D_e^2}, \qquad \widetilde{p}_\alpha = \frac{p_\alpha \varrho_e}{D_e^2}, \qquad \widetilde{\Phi} = \frac{2\Phi_0 L \varrho_e^2}{D_e^3}.$$

4.1 Assumptions upon parameters

We consider the low Mach number solution (3.17) for $(a, b) = (0, \alpha)$ and a certain unknown interfacial pressure p_α used as a boundary condition at $x = \alpha$. The density at the interface is thus equal to

$$\varrho_\alpha = \rho_\infty^{\mathrm{LM}}(\alpha) = \frac{\varrho_e}{1 + \frac{\Phi_0 \varrho_e \alpha}{\Upsilon D_e p_\alpha}} = \frac{\varrho_e}{1 + \frac{\widetilde{\Phi}}{2\Upsilon \widetilde{p}_\alpha}\frac{\alpha}{L}}. \tag{4.2}$$

We then consider the compressible solution (3.5) for $(a, b) = (\alpha, L)$ and ϱ_e replaced in (3.4–3.5) by ϱ_α.[4] The existence of this solution relies on the assumption (H1) adapted for the new set of parameters, *i.e.*

$$\frac{\Upsilon p_s \varrho_\alpha}{(\Upsilon - 1) D_e^2} > 1 + \sqrt{\frac{2\Phi_0 \varrho_\alpha^2 (L - \alpha)}{(2\Upsilon - 1) D_e^3}} \quad \Longleftrightarrow \quad \underbrace{\frac{\Upsilon}{\Upsilon - 1}\widetilde{p}_s - \sqrt{\frac{\widetilde{\Phi}}{2\Upsilon - 1}}\sqrt{\frac{L - \alpha}{L}} - 1 - \frac{\widetilde{\Phi}}{2\Upsilon \widetilde{p}_\alpha}\frac{\alpha}{L}}_{\mathcal{Q}(\alpha, \widetilde{p}_\alpha)} > 0. \tag{H_α}$$

A major remark is that p_∞ from (3.5) is monotone-decreasing. Consequently, we necessarily have

$$\widetilde{p}_\alpha \geq \widetilde{p}_s. \tag{4.3}$$

[4] $D_\alpha = D_e$ as the flow rate is constant in the low Mach number area.

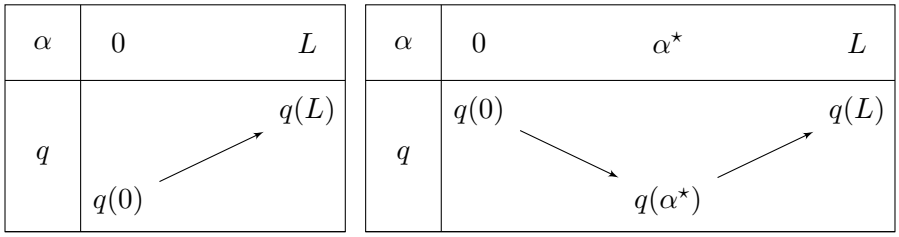

(a) Case $\alpha^\star < 0$ (b) Case $\alpha^\star \geq 0$

Figure 10: Variations of $q(\alpha) = \frac{\Upsilon}{\Upsilon-1}\widetilde{p}_s - \sqrt{\frac{\widetilde{\Phi}}{2\Upsilon-1}}\sqrt{\frac{L-\alpha}{L}} - 1 - \frac{\widetilde{\Phi}}{2\Upsilon\widetilde{p}_s}\frac{\alpha}{L}$

Since $\mathcal{Q}(\alpha,\cdot)$ is monotone-increasing, in order that (H_α) be satisfied, it is sufficient to ensure that $\mathcal{Q}(\alpha,\widetilde{p}_s) > 0$. This last requirement reads for α given in $(0,L)$

$$\widetilde{p}_s > \frac{\Upsilon-1}{2\Upsilon}\left[1 + \sqrt{\frac{\widetilde{\Phi}}{2\Upsilon-1}}\sqrt{\frac{L-\alpha}{L}} + \sqrt{\left(1+\sqrt{\frac{\widetilde{\Phi}}{2\Upsilon-1}}\sqrt{\frac{L-\alpha}{L}}\right)^2 + \frac{2\widetilde{\Phi}}{\Upsilon-1}\frac{\alpha}{L}}\right].$$

Notice that for $\alpha = 0$, we recover (H1).

However, as the position of α is not settled on and as we aim at highlighting the influence of α, we shall not make use of the inequality above and we enforce a more restrictive hypothesis upon $\widetilde{p}_s$ so that it does not depend on α, namely $\widetilde{p}_s$ is such that

$$\forall\, \alpha \in (0,L),\ q(\alpha) := \mathcal{Q}(\alpha,\widetilde{p}_s) > 0. \qquad (\mathrm{H}_{\widetilde{p}_s})$$

q is a $\mathscr{C}^1$-function over $(-\infty, L)$ with

$$q'(\alpha) = \frac{1}{2L}\sqrt{\frac{\widetilde{\Phi}}{(2\Upsilon-1)(1-\frac{\alpha}{L})}} - \frac{\widetilde{\Phi}}{2\Upsilon L\widetilde{p}_s}.$$

Two cases are thus to be considered depending on the sign of $\alpha^\star$ such that $q'(\alpha^\star) = 0$, *i.e.*

$$\alpha^\star = L\left(1 - \frac{\Upsilon^2\widetilde{p}_s^2}{(2\Upsilon-1)\widetilde{\Phi}}\right).$$

We mention that

$$\alpha^\star < 0 \iff \widetilde{p}_s > F_0(\widetilde{\Phi}) := \frac{2\Upsilon-1}{\Upsilon}\sqrt{\frac{\widetilde{\Phi}}{2\Upsilon-1}}.$$

- If parameters $\widetilde{p}_s$ and $\widetilde{\Phi}$ are such that $\alpha^\star < 0$ (see Figure 10a), ($\mathrm{H}_{\widetilde{p}_s}$) reduces to

$$q(0) > 0 \iff \widetilde{p}_s > F_-(\widetilde{\Phi}) := \frac{\Upsilon-1}{\Upsilon}\left(1+\sqrt{\frac{\widetilde{\Phi}}{2\Upsilon-1}}\right).$$

- Otherwise if $\alpha^\star \geq 0$ (see Figure 10b), ($\mathrm{H}_{\widetilde{p}_s}$) implies

$$q(\alpha^\star) = \frac{1}{2\widetilde{p}_s}\left(\frac{\Upsilon(3\Upsilon-1)}{(\Upsilon-1)(2\Upsilon-1)}\widetilde{p}_s^2 - 2\widetilde{p}_s - \frac{\widetilde{\Phi}}{\Upsilon}\right) > 0$$

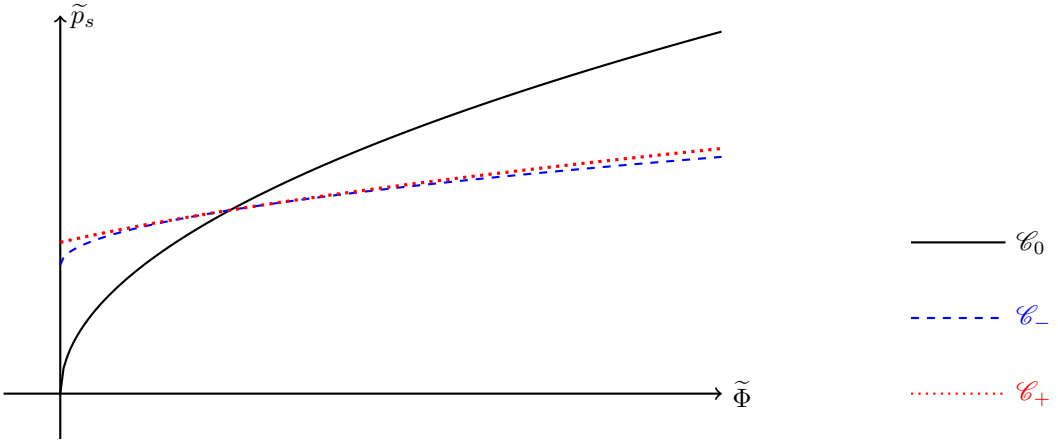

Figure 11: Constraints upon $\widetilde{p}_s$

or equivalently

$$\widetilde{p}_s > F_+(\widetilde{\Phi}) := \frac{\Upsilon-1}{\Upsilon}\frac{2\Upsilon-1}{3\Upsilon-1}\left(1+\sqrt{1+\frac{3\Upsilon-1}{(\Upsilon-1)(2\Upsilon-1)}\widetilde{\Phi}}\right).$$

Curves $\mathscr{C}_-$, $\mathscr{C}_0$ and $\mathscr{C}_+$ of functions F_-, F_0 and F_+ are depicted on Figure 11. Notice that these three curves intersect at the same point corresponding to $\widetilde{\Phi} = \frac{\Upsilon-1}{\Upsilon}\sqrt{2\Upsilon-1}$.

To sum up, ($\mathrm{H}_{\widetilde{p}_s}$) holds provided that

$$\widetilde{p}_s > \max\{F_-(\widetilde{\Phi}), F_0(\widetilde{\Phi})\} \qquad \text{or} \qquad F_+(\widetilde{\Phi}) < \widetilde{p}_s < F_0(\widetilde{\Phi}).$$

These inequalities reduce to

$$\widetilde{p}_s > F_\#(\widetilde{\Phi}) := \begin{cases} F_-(\widetilde{\Phi}), & \text{if } \widetilde{\Phi} \le \dfrac{\Upsilon-1}{\Upsilon}\sqrt{2\Upsilon-1}, \\ F_+(\widetilde{\Phi}), & \text{otherwise.} \end{cases} \tag{4.4}$$

Hence we can state that if parameters $\widetilde{p}_s$ and $\widetilde{\Phi}$ verify (4.4), (H_α) is satisfied for any $\alpha \in (0, L)$, which means that there exists a compressible steady state in (α, L) for any $\widetilde{p}_\alpha > \widetilde{p}_s$. Notice that in particular, if (4.4) holds, then we have $\widetilde{p}_s > F_-(\widetilde{\Phi})$ which is nothing but (H1): this ensures the existence of a compressible steady state over $(0, L)$. This state will be used as a reference state for comparisons.

Let us now get interested in the choice of $\widetilde{p}_\alpha$.

4.2 Computation of $\widetilde{p}_\alpha$

For now, we have constructed a steady state over $(0, L)$ made of a low Mach number part and a compressible part. This global steady state has by construction continuous density and velocity components but nothing is known about the pressure as the choice of p_α was free. To end up with the construction of the steady solution, we also impose the continuity of the pressure. More precisely, the transmission condition (2.9c) reads

$$p_\alpha = \frac{D_e^2}{\varrho_\alpha}\left[(\Upsilon-1)\left(1-\frac{\varrho_\alpha p_s}{D_e^2}\right)+\sqrt{\left(\Upsilon\frac{\varrho_\alpha p_s}{D_e^2}-\Upsilon+1\right)^2+2\frac{\Phi_0\varrho_\alpha^2(L-\alpha)}{D_e^3}}\right].$$

The right term is deduced from $\widetilde{p}_e$ (Prop. 2) adapted to new parameters (*i.e.* ϱ_α instead of ϱ_e). This equality is the steady counterpart of (4.1). Coming back to nondimensionalized notations and using the expression (4.2) for ϱ_α, the previous equality reads

$$\frac{\widetilde{p}_\alpha}{1+\frac{\widetilde{\Phi}}{2\Upsilon\widetilde{p}_\alpha}\frac{\alpha}{L}}-(\Upsilon-1)\left(1-\frac{\widetilde{p}_s}{1+\frac{\widetilde{\Phi}}{2\Upsilon\widetilde{p}_\alpha}\frac{\alpha}{L}}\right)=\sqrt{\left(\Upsilon\frac{\widetilde{p}_s}{1+\frac{\widetilde{\Phi}}{2\Upsilon\widetilde{p}_\alpha}\frac{\alpha}{L}}-\Upsilon+1\right)^2+\widetilde{\Phi}\frac{L-\alpha}{L}}.$$

Squaring both sides of the equality, we obtain after some algebra the following cubic equation

$$0=\widetilde{p}_\alpha^3+2(\Upsilon-1)(\widetilde{p}_s-1)\widetilde{p}_\alpha^2+\left[-(2\Upsilon-1)\widetilde{p}_s^2+2(\Upsilon-1)\widetilde{p}_s-\left(1-\frac{\alpha}{\Upsilon L}\right)\widetilde{\Phi}\right]\widetilde{p}_\alpha+\frac{\Upsilon-1}{\Upsilon}\frac{\alpha}{L}\widetilde{\Phi}\widetilde{p}_s. \quad (4.5)$$

Thus, we showed that deriving steady solutions for the overall coupled problem set in Section 2.3 comes down to solving a single algebraic equation whose solutions correspond to the interfacial pressure.

We denote by $\mathfrak{P}_\alpha$ the polynomial function (with respect to $\widetilde{p}_\alpha$) involved in the right hand side in (4.5). Let us mention first two algebraic remarks about $\mathfrak{P}_\alpha$:

❶ $\mathfrak{P}_\alpha$ admits three complex roots whose product is equal to $-\frac{\Upsilon-1}{\Upsilon}\frac{\alpha}{L}\widetilde{\Phi}\widetilde{p}_s<0$ (and at least one real root).

❷ $\mathfrak{P}_\alpha(\widetilde{p}_s)=-\left(1-\frac{\alpha}{L}\right)\widetilde{\Phi}\widetilde{p}_s<0$. As $\mathfrak{P}_\alpha(x)\xrightarrow{x\to+\infty}+\infty$, this shows that there exists at least one real root in the interval $(\widetilde{p}_s,+\infty)$.

Let us prove that there are exactly three real roots to this equation.

- If there were one real positive root and two complex conjugated roots (see Figure 12a), the product of these roots would be positive. This is contradictory with Remark ❶ above.
- If there were one double real negative root and one real positive root (see Figure 12b), the product would be positive which is still absurd.
- If there were one real negative root and one real double positive root (see Figure 12c), the function would be positive over $(0,+\infty)$ which is contradictory with the fact that $\mathfrak{P}_\alpha(\widetilde{p}_s)<0$ – see Remark ❷ above.
- In the 3 real root case, the roots can be located
  - either all of them in $(\widetilde{p}_s,+\infty)$ – see Figure 12d: this is impossible since the product would be positive;
  - or two of them in $(\widetilde{p}_s,+\infty)$ and one in $(-\infty,0)$ – see Figure 12e: this is not compatible with $\mathfrak{P}_\alpha(\widetilde{p}_s)<0$;
  - or one negative root, one lying in $(0,\widetilde{p}_s)$ and one lying in $(\widetilde{p}_s,+\infty)$ – see Figure 12f. This is the correct case.

Given (4.3), the value we are looking for is thus the largest root denoted $\widehat{\widetilde{p}}_\alpha>\widetilde{p}_s$. This shows the following lemma:

Lemma 3. *Under Hyp. (4.4), for any $\alpha\in(0,L)$, there exists a unique solution $\widehat{\widetilde{p}}_\alpha$ to equation (4.5) which corresponds to a physically admissible state.*

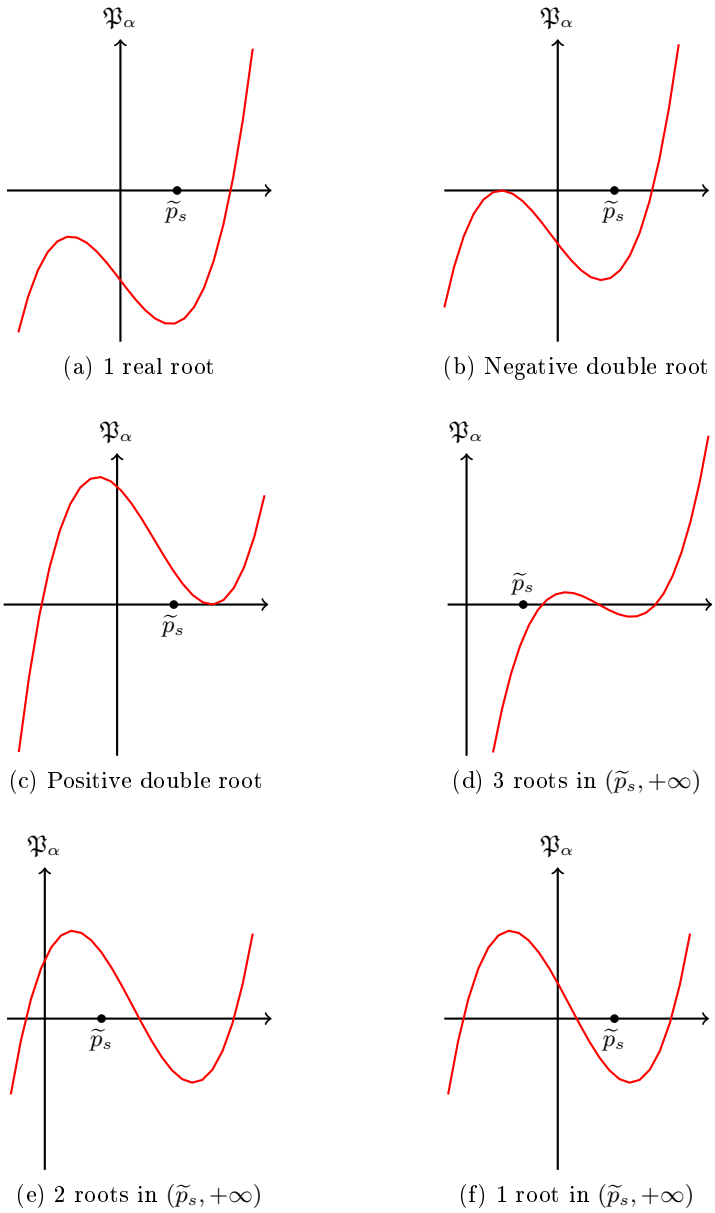

(a) 1 real root

(b) Negative double root

(c) Positive double root

(d) 3 roots in $(\widetilde{p}_s, +\infty)$

(e) 2 roots in $(\widetilde{p}_s, +\infty)$

(f) 1 root in $(\widetilde{p}_s, +\infty)$

Figure 12: Possible configurations for polynomial $\mathfrak{P}_\alpha$ (given that there is at least one root in $(\widetilde{p}_s, +\infty)$)

Notice that the Cardano's method yields some expressions for the three roots which are useless given their complexity. We provide some properties of this interfacial pressure and especially the influence of α. The proof of the following corollary is given in Appendix B.

Corollary 4. *Let us define the function* $\widetilde{p} : \alpha \mapsto \widehat{\widetilde{p}}_\alpha$.

1. $\widetilde{p}$ *is continuous and monotone-decreasing over* $(0, L)$.
2. $\widetilde{p}$ *varies between* $\widetilde{p}_s$ *and* $\widetilde{p}_e^+$.
3. *The reciprocal of* $\widetilde{p}$ *is defined over* $(\widetilde{p}_s, \widetilde{p}_e^+)$ *by*

$$\widetilde{p}^{-1}(p) = \frac{\Upsilon L}{\widetilde{\Phi}} \frac{p(\widetilde{p}_e^+ - p)(p - \widetilde{p}_e^-)}{p + (\Upsilon - 1)\widetilde{p}_s}.$$

In conclusion, we managed to construct a unique steady solution of the coupled problem set in Section 2.3 through the chosen transmission conditions:

Proposition 4. *Under hypothesis* (4.4)*, there exists a unique physical steady solution to the coupled problem between System* (2.5) *over* $(0, \alpha)$ *with BC* (2.8a-2.8b) *and System* (2.4) *over* (α, L) *with BC* (2.8c) *through transmission conditions* (2.9).

Of course, this result does not prove the well-posedness of this model. This rather hints that the coupling strategy (2.9) is relevant in the steady case.

Remark 6. *Although this coupled steady state is continuous, it is never of class* $\mathscr{C}^1(0, L)$*. Indeed, we find out that*

$$\frac{[\rho_\infty^{\mathrm{LM}}]'(\alpha)}{[\rho_\infty]'(\alpha)} = \frac{L - \alpha}{L} \frac{\Upsilon \widehat{\widetilde{p}}_\alpha - \Upsilon + 1}{\Upsilon \widehat{\widetilde{p}}_\alpha + \frac{\alpha \widetilde{\Phi}}{2L}} \neq 1.$$

5 Numerical strategies

This section is devoted to the simulation of unsteady solutions of the coupled problem (2.4–2.5) with IC (2.7), BC (2.8) and transmission conditions (2.9). Several strategies can be contemplated: a first one would consist in applying the same scheme in the whole domain and to project the solution onto a relevant space (constant thermodynamic pressure $\mathcal{P}$ and velocity field such that $\partial_x u - \Phi/(\Upsilon\mathcal{P})$ is constant) through a relaxation approach. This will not be studied in this paper. A second method relies on the coupling of two different schemes dedicated to the two specific regimes.

The domain $(0, L)$ is discretized by means of a homogeneous Cartesian grid $x_{i-1/2} = (i-1)\Delta x$, $1 \leq i \leq N$, $\Delta x = \frac{L}{N-1}$ for some $N \in \mathbb{Z}_+^*$. The cell $(x_{i-1/2}, x_{i+1/2})$ is named $\mathcal{C}_i$ and its center is denoted by x_i.

As for the time discretization, let $\Delta t^n > 0$ be the n-th time step to be determined later and $t^{n+1} = t^n + \Delta t^n$. In the framework of finite volume methods, $*_i^n$ denotes the value of variable $*$ at time t^n and cell $\mathcal{C}_i$.

This part is organized as follows. As in the theoretical section, we first focus on the two specific schemes separately (§ 5.1). The very coupling is studied after (§ 5.2).

5.1 Dedicated schemes

5.1.1 Compressible scheme

The hyperbolic system of conservation laws with source term (2.4) supplemented with BC (2.6) over $(a,b)=(0,L)$ is classically discretized by means of a 1st-order explicit finite-volume method

$$\mathbf{W}_i^{n+1} = \mathbf{W}_i^n - \frac{\Delta t^n}{\Delta x}\left(\mathcal{F}(\mathbf{W}_i^n, \mathbf{W}_{i+1}^n) - \mathcal{F}(\mathbf{W}_{i+1}^n, \mathbf{W}_i^n)\right), \tag{5.1}$$

where unknowns are located at the center of the cells. The numerical flux $\mathcal{F}$ is any consistant, homogeneous and Lipschitz-continuous flux stable under the CFL condition

$$\Delta t \leq \frac{\mathcal{C}_{CFL}\cdot\Delta x}{\lambda(\mathbf{W}_\ell, \mathbf{W}_r)}.$$

In the sequel, we choose $\mathcal{C}_{CFL}=0.5$ and $\lambda(\mathbf{W}_\ell,\mathbf{W}_r)=\max\{|u_\ell|+c_\ell, |u_r|+c_r\}$. The choice of the numerical flux (and the analysis of the corresponding scheme) is not the topic of this paper and is thus left to the reader. All simulations in the sequel are performed by means of the Rusanov scheme.

5.1.2 Low Mach scheme

To simulate System (2.5) with BC (2.6) over $(a,b)=(0,L)$, we use a staggered grid (ρ and π are located at the center of the cells and u at the boundaries of the cells) like in the MAC scheme for incompressible fluids [23]. We decouple the equations thanks to an explicit strategy. Knowing Δt^n, $(\rho_i^n)_{1\leq i\leq N-1}$, $(u_{i-1/2}^n)_{1\leq i\leq N}$, $(\pi_i^n)_{1\leq i\leq N-1}$ and $\mathcal{P}^n$, the algorithm reads

① ρ^{n+1} is computed by means of a standard finite-volume formulation

$$\rho_i^{n+1} = \rho_i^n - \frac{\Delta t^n}{\Delta x}\left[f_{i+1/2}^n(\rho_i^n,\rho_{i+1}^n) - f_{i-1/2}^n(\rho_{i-1}^n,\rho_i^n)\right];$$

② $\mathcal{P}^{n+1}$ is prescribed by the boundary condition: $\mathcal{P}^{n+1}=\mathcal{P}_s(t^{n+1})$;

③ Depending of the availability of the data, we compute either the exact value of $\mathcal{P}_s'(t^{n+1})$ or an approximation (for instance by means of an explicit 1st-order scheme $\frac{\mathcal{P}^{n+1}-\mathcal{P}^n}{\Delta t^n}$) denoted by $[\mathcal{P}']^{n+1}$;

④ The velocity is computed by a direct integration of (2.5b)

$$u_{i-1/2}^{n+1} = \mathfrak{u}_e(t^{n+1}) - \frac{\Upsilon-1}{\Upsilon}\frac{[\mathcal{P}']^{n+1}}{\mathcal{P}^{n+1}}x_{i-1/2} + \frac{1}{\Upsilon\mathcal{P}^{n+1}}\int_0^{x_{i-1/2}}\Phi(x)\,\mathrm{d}x.$$

The choice of the numerical flux $f_{i+1/2}^n$ is free and may be imposed by conservativity considerations (see below). However, we choose for the subsequent simulations the upwind flux

$$f_{i-1/2}^n(\rho_\ell,\rho_r) = \begin{cases}\rho_\ell u_{i-1/2}^n, & \text{if } u_{i-1/2}^n \geq 0,\\ \rho_r u_{i-1/2}^n, & \text{if } u_{i-1/2}^n < 0.\end{cases}$$

It is stable under the CFL condition

$$\Delta t \leq \frac{\mathcal{C}_{CFL}\cdot\Delta x}{\|u\|_\infty}.$$

In that case, it is possible to determine the asymptotic numerical state (assuming $\mathfrak{u}_e$ and $\mathcal{P}_s$ converge to $\bar{\mathfrak{u}}_e$ and p_s as $t \to +\infty$). According to Step ④, we have

$$u^{\infty}_{i+1/2} = \bar{\mathfrak{u}}_e + \frac{1}{\Upsilon p_s} \int_0^{x_{i+1/2}} \Phi(x)\, \mathrm{d}x = u^{\mathrm{BM}}_{\infty}(x_{i+1/2}) > 0.$$

Then, the asymptotic numerical density is deduced from Step ① with the upwind flux:

$$\rho^{\infty}_i u^{\infty}_{i+1/2} = \rho^{\infty}_{i-1} u^{\infty}_{i-1/2} = D_e \quad \Longrightarrow \quad \rho^{\infty}_i = \frac{D_e}{u^{\infty}_{i+1/2}} = \rho^{\mathrm{BM}}_{\infty}(x_{i+1/2}) = \rho^{\mathrm{BM}}_{\infty}(x_i) + \mathcal{O}(\Delta x).$$

The consistency error comes for the staggering procedure in the mesh.

5.1.3 Comparisons

We compare the two schemes proposed in the previous sections by simulating a situation where the asymptotic Mach number is small, namely Case 1. (§ 3.2.3). Corresponding steady states (for the low Mach and the compressible models) are very close as shown on Figure 15.

We represent on Figure 13a the compressible steady state as well as the numerical solutions obtained by means of the compressible (§ 5.1.1) and low Mach (§ 5.1.2) schemes with $N = 51$. The initial conditions are $u^0(x) = \mathfrak{u}_e + 10x$, $\rho^0(x) = \varrho_0$ and $p^0(x) = p_s$. Although the Mach number is small asymptotically, it is not the case all along the simulation (about 0.2 at the beginning with this set of initial data).

At time $t = 0.5$ s, the numerical solutions do not evolve anymore. We observe that the steady state seems to be an asymptotic state as both numerical solutions got closer. However, the asymptotic numerical solution provided by the compressible solver is much less accurate than its low Mach counterpart. The accuracy is investigated on Figure 13b. As expected, the low Mach scheme is much more efficient (≈ 380 iterations to reach the asymptotics) than the compressible solver (≈ 4580 iterations). This is due to the respective CFL conditions.

We notice that there is no (acoustic) oscillation for the low Mach scheme which is accounted for by the fact that the acoustic waves have been filtered out in the derivation of the model. On the contrary, oscillations occur for the compressible pressure (but not for the density) which oscillates around the steady state.

Thus, the low Mach solver in a low Mach regime turns out to be both accurate and efficient with a higer rate of convergence towards the asymptotic state. The unsteady behaviour may lack in physical content but this provides a reliable approximation.

5.2 Design of a stable coupling algorithm

We now derive a strategy to couple the two numerical states constructed previously. A first strategy would consist in applying what is described at the beginning of Section 4, *i.e.* in solving the fixed-point problem (4.1) at each time iteration but this seems to be expensive from a computational point of view. We rather simulate the models with an explicit handling of the transmission conditions. In the sequel, the resulting scheme is referred to as the hybrid scheme.

We first investigate the case where $\alpha(t) = \alpha_0$. α_0 is chosen so that the steady Mach number associated to the steady solution (3.5) satisfies

$$\mathcal{M}_{\infty}(x) \begin{cases} < \mathcal{S} & \text{for } x \in (0, \alpha_0), \\ > \mathcal{S} & \text{for } x \in (\alpha_0, L), \end{cases}$$

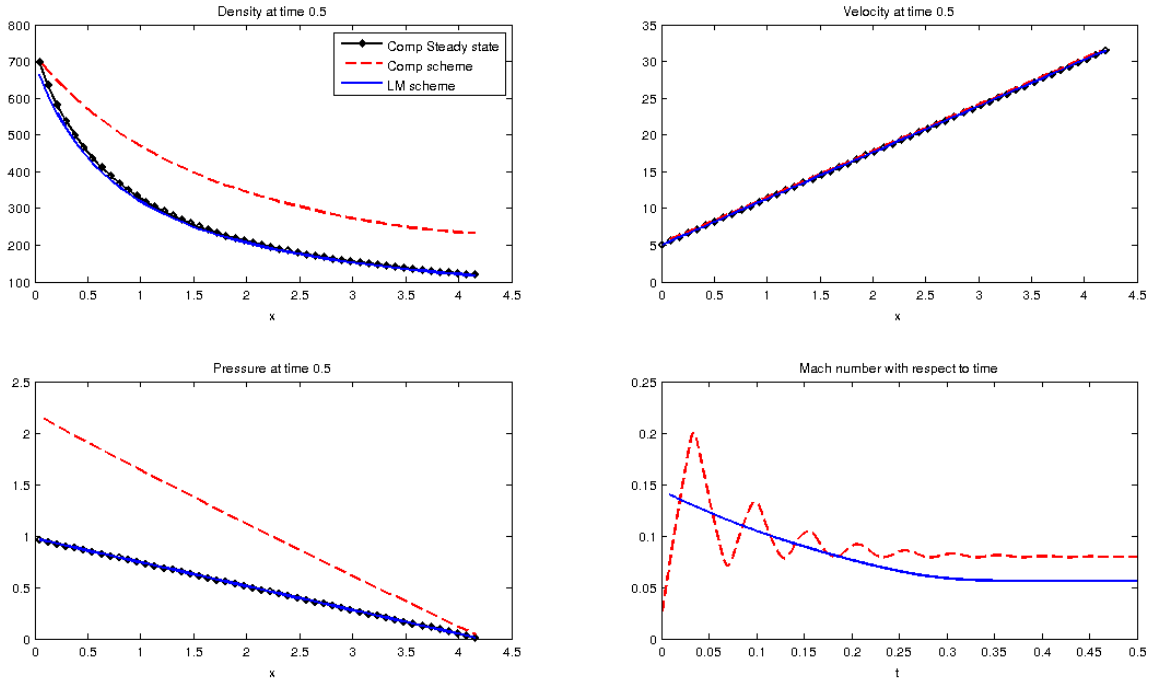

(a) Graphs of density, velocity, pressure and Mach number

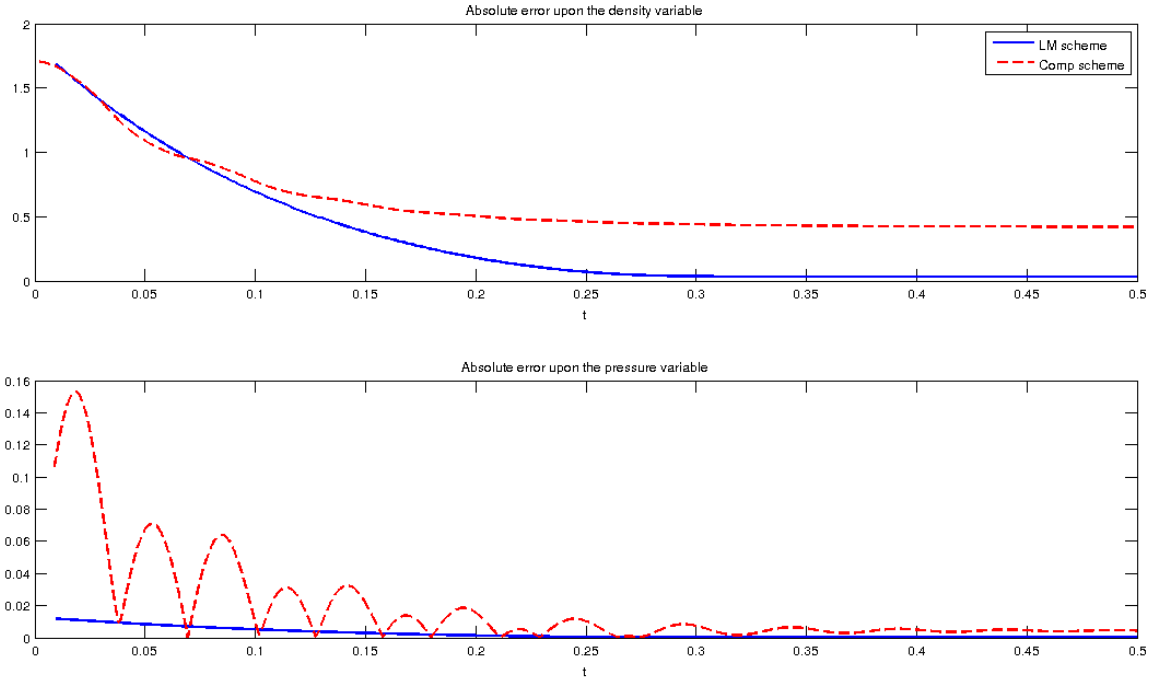

(b) Graphs of absolute errors with respect to the asymptotic state

Figure 13: Comparisons of the compressible (§ 5.1.1) and the low Mach (§ 5.1.2) schemes in a low Mach number regime

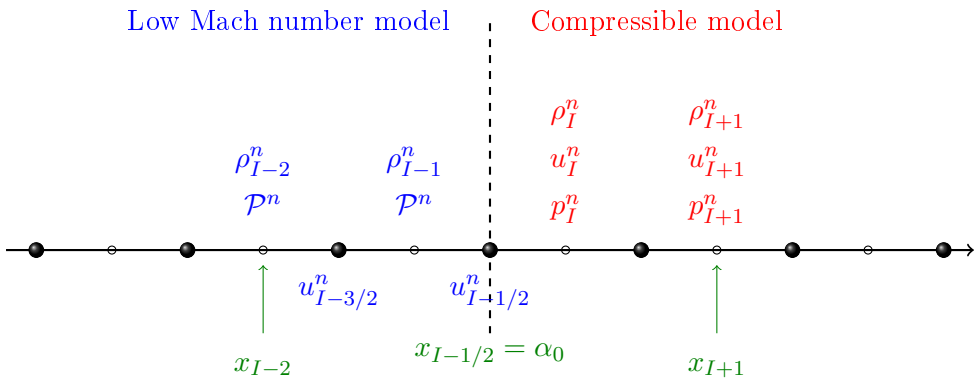

Figure 14: Location of numerical unknowns

where $\mathcal{S}$ is the threshold under which the low Mach number assumption is valid.

Let $I := 1 + \frac{\alpha_0}{\Delta x}$ be the index of the first cell of the compressible domain – see Figure 14. α_0 is set such that $\frac{\alpha_0}{\Delta x}$ is an integer.[5]

Low Mach and compressible variables are located as prescribed in the design of specific schemes (see § 5.1 and Figure 14).

Let us assume we are given $(u^n_{i-1/2})_{1\leq i\leq I}$, $(\rho^n_i, \pi^n_i)_{1\leq i\leq I-1}$, $\mathcal{P}^n$ and $(\mathbf{W}^n_i)_{I\leq i\leq N-1}$. On the one hand, the explicitness of the scheme enables to deal with the compressible part first. On the other hand, it is necessary to handle this part first as the low Mach computation requires $\mathcal{P}^{n+1}$ and/or $u^{n+1}_{I-1/2}$. The algorithm that we propose thereby reads as follows:

① We first solve (2.4) by means of the 1st-order finite-volume method (5.1) over $[\alpha_0, L]$.

The handling of the boundary conditions must now be specified. Two possibilities arise similarly to the modelling of interfaces described in the introduction:

(a) Either we consider that the compressible domain is the very prolongation of the low Mach number domain which means that Scheme (5.1) naturally applies to cell $\mathcal{C}_I$ with

$$\mathcal{F}^n_{I-1/2} = \mathcal{F}(\widetilde{\mathbf{W}}^n_{I-1}, \mathbf{W}^n_I) \qquad \text{and} \qquad \widetilde{\mathbf{W}}^n_{I-1} = \mathcal{W}\left(\rho^n_{I-1}, \frac{u^n_{I-3/2} + u^n_{I-1/2}}{2}, \mathcal{P}^n\right). \tag{5.2a}$$

(b) Or we consider $x = \alpha_0$ as a kind of boundary and we use the spirit of [14]. More precisely, the transmission between the two subdomains is achieved by setting

$$\mathcal{F}^n_{I-1/2} = \mathcal{F}(\widehat{\mathbf{W}}^n_{I-1}, \mathbf{W}^n_I) \qquad \text{and} \qquad \widehat{\mathbf{W}}^n_{I-1} = \mathcal{W}\left(\rho^n_{I-1}, \frac{u^n_{I-3/2} + u^n_{I-1/2}}{2}, 2p^n_I - p^n_{I+1}\right) \tag{5.2b}$$

to take into account the sign of eigenvalues of the hyperbolic problem: this strategy corresponds to the resolution of the Euler equations (2.4) in (α_0, L) together with boundary conditions for ρ and u at $x = \alpha_0$ and for p at $x = L$.

As for the handling of the boundary conditions at the exit of the domain, it is a major numerical issue. Indeed, to get an accurate value of the numerical outlet pressure, an analysis of the compressible scheme must be carried out but it is not the topic of this paper (see [14]).

[5] We assume that α_0 is rational which is not restrictive as α_0 is a modelling parameter.

② We then handle the low Mach number subdomain. To solve the transport equation (2.5a) over (t^n, t^{n+1}), we use an implicit or explicit standard scheme (which can be compatible with the one used in Step ① if one wants to ensure the conservation of mass) or a numerical method of characteristics (using the nonconservative formulation – see [40]). The time step induced by the previous stage is still convenient for the present one since there is only a material wave (slower than the acoustic wave in this context). For the boundary conditions, values for $\tilde{\rho}_{I-1/2}$ are available at time t^n and t^{n+1} and may be used depending on the explicitness of the scheme.

According to (2.9c), we compute the new thermodynamic pressure by the 2nd-order interpolation formula $\mathcal{P}^{n+1} = \dfrac{3p_I^{n+1} - p_{I+1}^{n+1}}{2}$. To compute the velocity, we would like to apply the same procedure as in § 5.1.2, which requires an approximation of $\mathcal{P}'(t^{n+1})$. Attempts to approximate this quantity by means of finite-difference formulae turned out to lead to numerical instabilities. That is why it is necessary to apply a different approach.

Our algorithm relies on the compatibility equation (2.3). Setting $\tilde{u}_{I-1/2}^{n+1} := \frac{1}{2}\left(3u_I^{n+1} - u_{I+1}^{n+1}\right)$ which is computed thanks to the compressible step, we compute

$$\eta^{n+1} := \frac{1}{\alpha_0}\left(\tilde{u}_{I-1/2}^{n+1} - \mathfrak{u}_e(t^{n+1}) - \frac{1}{\Upsilon\mathcal{P}^{n+1}}\int_0^{\alpha_0}\Phi(x)\,\mathrm{d}x\right) \approx -\frac{(\Upsilon-1)\mathcal{P}'}{\Upsilon\mathcal{P}}(t^{n+1}). \tag{5.3}$$

Hence

$$u_{i-1/2}^{n+1} = \mathfrak{u}_e(t^{n+1}) + \eta^{n+1}x_{i-1/2} + \frac{1}{\Upsilon\mathcal{P}^{n+1}}\int_0^{x_{i-1/2}}\Phi(x)\,\mathrm{d}x.$$

This strategy turned out to provide stable results which are shown in the following section.

We do not mention the computation of π since in dimension 1, the momentum equation (2.5c) is decoupled from the other equations and is thus only a postprocessing for π.

The position of the interface α_0 is arbitrary and could imply additional numerical errors. Even if is legitimate for large times as it is based upon the steady Mach number, it can be no longer the case for short times. Indeed, the Mach number can be large in the unsteady regime and a fixed interface may not be relevant. That is why we get interested in a moving interface approach. α^n is tuned by the levet set equal to a given threshold $\mathcal{S}$ of the current Mach number $\mathcal{M}_i^n$ computed in each cell.

The algorithm detailed above can directly be adapted. Index I^n is updated at each time step. At the end of each iteration, the current conservative state is reconstructed in both subdomains. In particular, in the low Mach domain, we set $\mathbf{W}_i^n = \mathcal{W}\left(\rho_i^n, \frac{u_{i-1/2}^n + u_{i+1/2}^n}{2}, \mathcal{P}^n\right)$. In the computation of η^{n+1}, an explicit handling is achieved by replacing α_0 in (5.3) by α^n and I by I^n.

5.3 Numerical results

We focus on a configuration where the steady state is not entirely in the low Mach regime. Compared to the standard data of Case 1., Φ_0 is increased and p_s decreased. Steady solutions are depicted on Figure 15a. The Mach number ranges from 0.04 to 0.23 and we observe that the velocity is over-estimated under the low Mach approximation.

The compressible scheme (§ 5.1.1) and the hybrid strategy (§ 5.2) are applied to this case and results are compared on Figure 15b. The hybrid scheme is assessed both in the fixed and the moving interface setup. We first mention that strategies (5.2a) and (5.2b) provide quite similar results in the fixed interface case but the pure low Mach flux (5.2a) induces oscillations of the interface when the latter is no longer fixed. That is why we recommend the use of strategy (5.2b). Secondly, we do not observe any

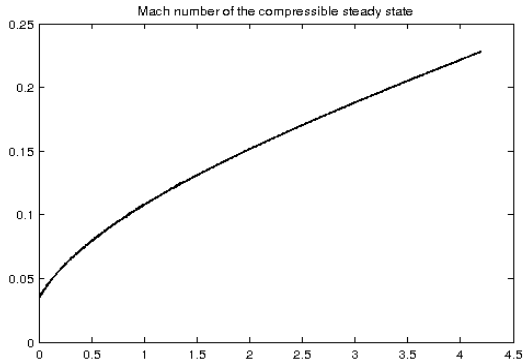

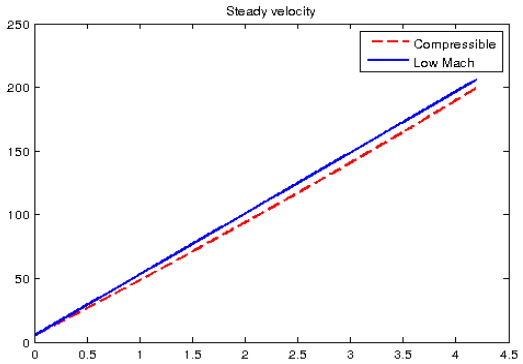

(a) Steady states profiles

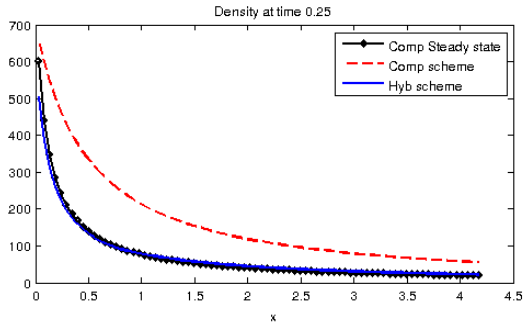

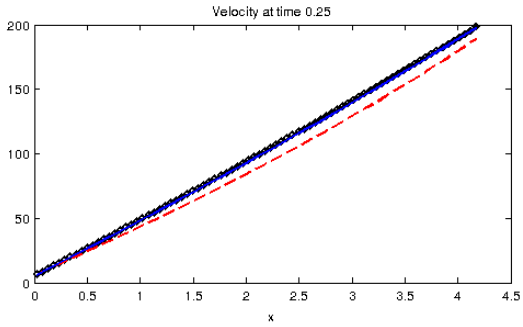

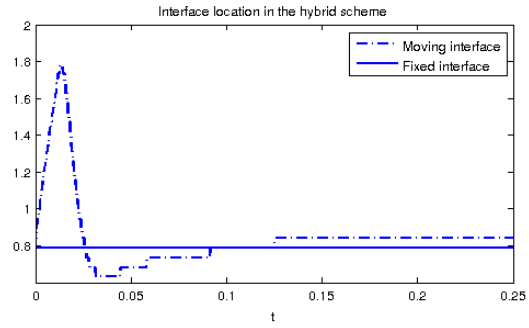

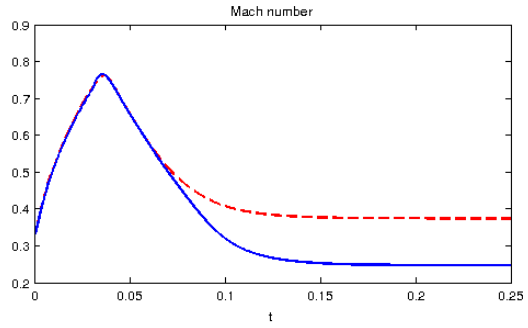

(b) Asymptotic numerical states

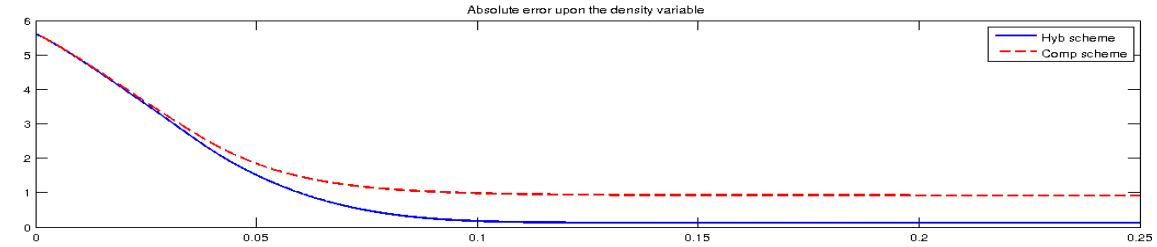

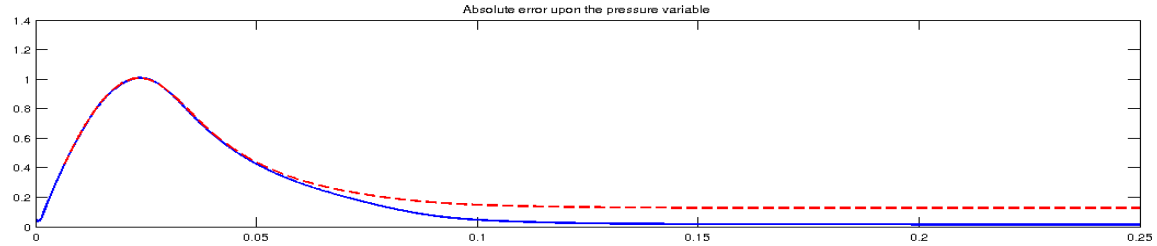

(c) Numerical errors

Figure 15: Case 5. $\Phi_0 = 5 \cdot 10^8\,\mathrm{W}\cdot\mathrm{m}^{-3}$, $p_s = 6 \cdot 10^6\,\mathrm{Pa}$

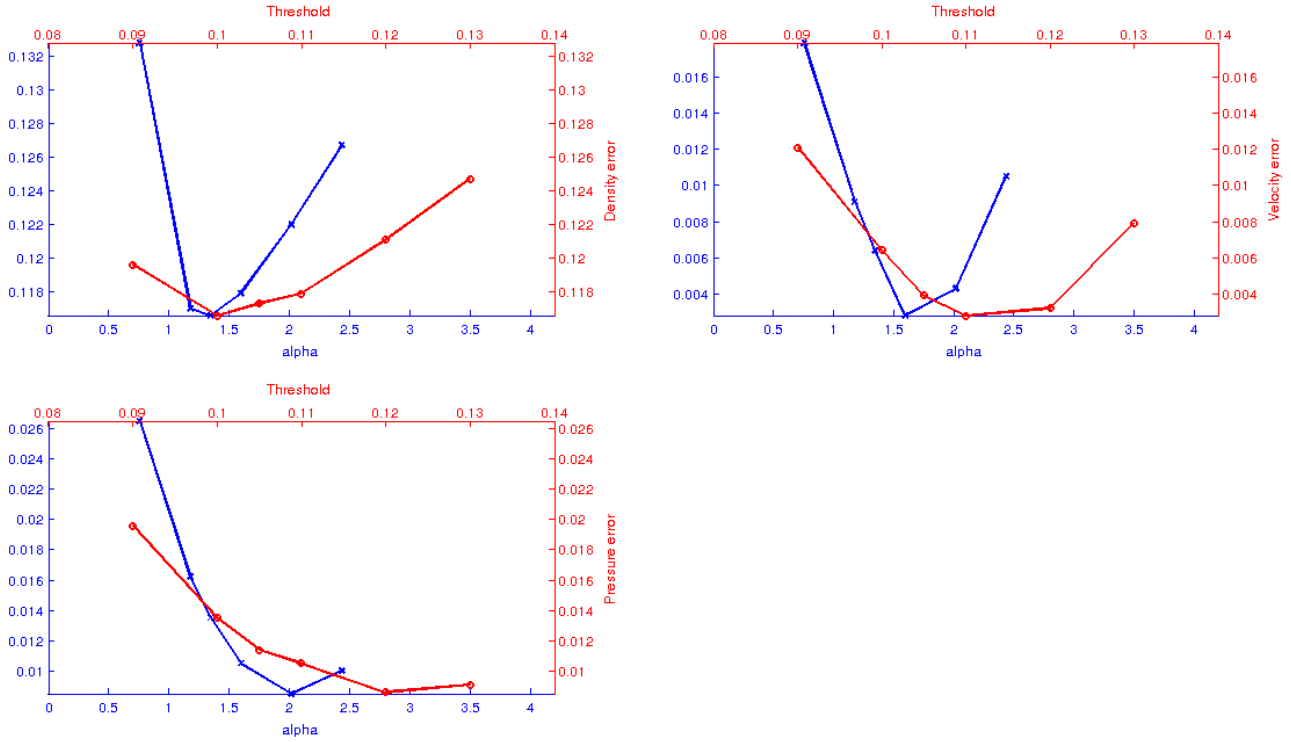

Figure 16: Influence of parameters α_0 (crosses) and $\mathcal{S}$ (circles) upon the numerical errors (density, velocity, pressure)

noticeable difference between results for the fixed and moving interface approaches at convergence (in time). Making the interface evolves seems more relevant in the unsteady regime as the Mach number increases till 0.9 in the course of the computation.

Compared to the compressible scheme, the hybrid strategy is much more accurate (see Figure 15c) although it only differs over a small part of the domain, *i.e.* a quarter of the domain with $\alpha_0 = 0.8$. We recall that the scheme is the same in the other part.

Sensitivity of the numerical errors with respect to the parameters of the hybrid strategies (α_0 if fixed, $\mathcal{S}$ if moving) is investigated on Figure 16. We clearly observe that in both studies, a minimum can be reached for each variable (density, velocity and pressure) but not with the same minimizer. It is then hard to determine a priori the best value for α_0 or $\mathcal{S}$. The error can be multiplied by 2, 3 or 4 depending on the value of the parameter. However, tuning $\mathcal{S}$ to 0.1 seems to be a good compromise as seen on Figure 9.

6 Conclusion

1D computations of fluid flows have been investigated in this work considering the influence of the Mach number upon the robustness of the underlying scheme. Compressible schemes may present difficulties to converge in time when the Mach number becomes small. That is why we developed a coupling strategy to incorporate specificities of Mach regimes.

We first focused on a low Mach model which offers many advantages compared to the compressible system it is resulting from: it is possible to derive explicit expressions for both steady and unsteady cases, numerical solutions are accurate in the steady regime and the corresponding algorithm is efficient due to a less restrictive stability condition. The link between steady solutions of both models is then

studied in order to better understand the influence of the Mach number.

Secondly, we got interested in configurations where the low Mach hypothesis does not hold in the whole domain of computation for physical reasons. To deal with this issue, we proposed a coupling approach which relies on the resolution of each model in its relevant domain together with transmission conditions through the interface. This strategy turned out to provide a global steady state for the coupling problem and a robust algorithm which forms a first stage in the study of low Mach – compressible flows. Notice that the inaccuracy of compressible solvers is not investigated in the present work (see [14]).

Several perspectives must however be examined in future works. First of all, we must make the code robust to appearances/disappearances of a regime as the results above only concern situations where both models are present throughout the computation. Second of all, the handling of time steps must be improved. Indeed, the acoustic CFL condition is imposed in the low Mach domain which is not necessary. The efficiency can thus be enhanced by means of a subcycling strategy (material time step in the low Mach domain, acoustic time step in the compressible part). Third of all, this approach must be extended to dimension 2. Two issues are raised: on the one hand, the continuity condition imposed on the thermodynamic pressure is no more valid in 2D as it is constant on one side of the interface and variable all along the other side. On the other hand, the decoupling between the momentum equation and the others does not hold anymore and the computation of the dynamic pressure becomes a major point.

A Derivation of Formulae

A.1 Equality (3.9b)

From (3.9a), we have

$$\begin{aligned}\frac{\varrho_e}{\rho_\infty(x)} &= \frac{2\Upsilon\widetilde{p}_e + 1 + \widetilde{\Phi}\frac{x-a}{b-a}}{\Upsilon(\widetilde{p}_e+1) \pm \sqrt{(\Upsilon\widetilde{p}_e - \Upsilon + 1)^2 - (2\Upsilon-1)\widetilde{\Phi}\frac{x-a}{b-a}}} \\ &= \frac{\left(2\Upsilon\widetilde{p}_e + 1 + \widetilde{\Phi}\frac{x-a}{b-a}\right)\left(\Upsilon(\widetilde{p}_e+1) \mp \sqrt{(\Upsilon\widetilde{p}_e - \Upsilon + 1)^2 - (2\Upsilon-1)\widetilde{\Phi}\frac{x-a}{b-a}}\right)}{\Upsilon^2(\widetilde{p}_e+1)^2 - (\Upsilon\widetilde{p}_e - \Upsilon + 1)^2 + (2\Upsilon-1)\widetilde{\Phi}\frac{x-a}{b-a}} \\ &= \frac{1}{2\Upsilon-1}\left(\Upsilon(\widetilde{p}_e+1) \mp \sqrt{(\Upsilon\widetilde{p}_e - \Upsilon + 1)^2 - (2\Upsilon-1)\widetilde{\Phi}\frac{x-a}{b-a}}\right).\end{aligned}$$

Hence, from (3.7b'), we deduce (3.9b).

A.2 Equality (3.13)

As $\mathcal{X}_s = \Upsilon - \Upsilon\widetilde{p}_s - 1$, we deduce from the expression (3.11) of $\widetilde{p}_e^{\pm}$ that

$$\begin{aligned}&(\Upsilon\widetilde{p}_e - \Upsilon + 1)^2 - (2\Upsilon-1)\widetilde{\Phi} \\ &\qquad = \left[\Upsilon(\Upsilon-1)(1-\widetilde{p}_s) \pm \Upsilon\sqrt{\mathcal{X}_s^2 + \widetilde{\Phi}} - (\Upsilon-1)\right]^2 - (2\Upsilon-1)\widetilde{\Phi} \\ &\qquad = \Upsilon^2\mathcal{X}_s^2 + (\Upsilon-1)^2(\mathcal{X}^2 + \widetilde{\Phi}) \pm 2\Upsilon(\Upsilon-1)\mathcal{X}_s\sqrt{\mathcal{X}_s^2 + \widetilde{\Phi}} \\ &\qquad = \left[\Upsilon\mathcal{X}_s \pm (\Upsilon-1)\sqrt{\mathcal{X}_s^2 + \widetilde{\Phi}}\right]^2.\end{aligned}$$

B Proof of Corollary 4

In the sequel, we note

$$\mathfrak{P}_\alpha = X^3 + \varepsilon_2 X^2 + (\alpha\varepsilon_{11} + \varepsilon_{10})X + \alpha\varepsilon_0$$

where $\varepsilon_2 := 2(\Upsilon-1)(\widetilde{p}_s - 1)$, $\varepsilon_{10} := -(2\Upsilon-1)\widetilde{p}_s^2 + 2(\Upsilon-1)\widetilde{p}_s - \widetilde{\Phi}$, $\varepsilon_{11} := \frac{\widetilde{\Phi}}{\Upsilon L}$ and $\varepsilon_0 := \frac{\Upsilon-1}{\Upsilon}\frac{\widetilde{\Phi}\widetilde{p}_s}{L}$.

Continuity of polynomial roots with respect to their coefficients[6] have been long studied in the literature (see for instance [30, Ch. V] and [34, Th. 1.4]). These results ensure the continuity of the three complex roots of (4.5) with respect to α. The issue is rather to determine whether these roots remain real or not. As $\mathfrak{P}_\alpha$ is a 3rd-degree polynomial with real coefficients, it has either 0 or 2 nonreal roots which must be conjugated. By continuity, the transition between these 2 configurations is the case where there is a double root, *i.e.* when $\widetilde{p}_\alpha$ is a root of both $\mathfrak{P}_\alpha$ and $\mathfrak{P}'_\alpha$. As we concluded in § 4.2, situations from Figures 12b and 12c cannot happen for $\alpha \in (0, L)$.

The same conclusion arises with the application of the implicit function theorem. Let α_0 be a number in $(0, L)$. Eq. (4.5) also reads

$$\mathfrak{P}\big(\alpha_0, \widetilde{p}(\alpha_0)\big) := \mathfrak{P}_{\alpha_0}\left(\widehat{\widetilde{p}}_{\alpha_0}\right) = 0.$$

The existence of such an implicit function $\widetilde{p}$ results from the fact that $\partial_p\mathfrak{P}(\alpha_0, \cdot) \neq 0$ in the vicinity of $\widehat{\widetilde{p}}_{\alpha_0}$. This is the case because $\partial_p\mathfrak{P}\big(\alpha_0, \widetilde{p}(\alpha_0)\big) = \mathfrak{P}'_{\alpha_0}\left(\widehat{\widetilde{p}}_{\alpha_0}\right) > 0$ according to Figure 12f. Hence the continuity over $(0, L)$. Moreover, $\widetilde{p}$ is of class $\mathscr{C}^1$ as $\partial_\alpha\mathfrak{P}(\alpha_0, \cdot) > 0$ with

$$\widetilde{p}'(\alpha_0) = -\frac{\partial_\alpha\mathfrak{P}\big(\alpha_0, \widetilde{p}(\alpha_0)\big)}{\partial_p\mathfrak{P}\big(\alpha_0, \widetilde{p}(\alpha_0)\big)} = -\frac{\varepsilon_{11}\widetilde{p}(\alpha_0) + \varepsilon_0}{3\widetilde{p}(\alpha_0)^2 + 2\varepsilon_2\widetilde{p}(\alpha_0) + \varepsilon_{11}\alpha + \varepsilon_{10}} < 0$$

from which we infer that $\widetilde{p}$ is monotone-decreasing.

Critical cases are thus $\alpha = 0$ and $\alpha = L$. First of all, for $\alpha = 0$ (which corresponds to the fully compressible case), we remark that

$$\mathfrak{P}_0 = X\left[X^2 + 2(\Upsilon-1)(\widetilde{p}_s - 1)X + \left(-(2\Upsilon-1)\widetilde{p}_s^2 + 2(\Upsilon-1)\widetilde{p}_s - \widetilde{\Phi}\right)\right].$$

As $\widetilde{p}_0 \neq 0$, Equation (4.5) is then nothing but the equation satisfied by $\widetilde{p}_e$ for the Euler system – see Eq. (3.10). The 3 roots are 0, $\widetilde{p}_e^-$ and $\widetilde{p}_e^+ > \max\{\widetilde{p}_e^-, 0\}$. Then $\widetilde{p}(0) = \widetilde{p}_e^+$: we recover exactly the result from Prop. 2 as expected and $\widetilde{p}$ is continuous at $\alpha = 0$.

Secondly, for $\alpha = L$, we have

$$\mathfrak{P}_L = (X - \widetilde{p}_s)\left[X^2 + \big((2\Upsilon-1)\widetilde{p}_s - 2(\Upsilon-1)\big)X - \frac{\Upsilon-1}{\Upsilon}\widetilde{\Phi}\right].$$

This equation admits three roots: one negative and two positive (among which $\widetilde{p}_s$). The reasoning that lead to the existence of $\widehat{\widetilde{p}}_\alpha$ no longer holds since in that case $\mathfrak{P}(\widetilde{p}_s) = 0$. To prove that $\widetilde{p}(\alpha)$ actually converges to $\widetilde{p}_s$, we must prove that $\widetilde{p}_s$ is the largest root of the equation above. We notice that

$$\mathfrak{P}'_L(\widetilde{p}_s) = 2\Upsilon\widetilde{p}_s^2 - 2(\Upsilon-1)\widetilde{p}_s - \frac{\Upsilon-1}{\Upsilon}\widetilde{\Phi}.$$

Hence $\mathfrak{P}'_L(\widetilde{p}_s) > 0$ is equivalent to $\widetilde{p}_s > F_L(\widetilde{\Phi})$ where

$$F_L(\widetilde{\Phi}) := \frac{\Upsilon-1}{\Upsilon}\frac{1 + \sqrt{1 + \frac{2\widetilde{\Phi}}{\Upsilon-1}}}{2}.$$

[6] Which are themselves 1st-degree polynomials wrt α in the present case.

We can check that $F_L(\widetilde{\Phi}) < F_\#(\widetilde{\Phi})$ for all $\widetilde{\Phi} > 0$ – see Appendix C. Hence, under Hyp. (4.4), $\widetilde{p}_s > F_L(\widetilde{\Phi})$ and $\mathfrak{P}_L$ is monotone-increasing in the vicinity of $p = \widetilde{p}_s$ which implies that $\widetilde{p}_s$ is the largest root. The limit of $\widetilde{p}(\alpha)$ when $\alpha \to L$ is thus $\widetilde{p}_s$: this is in accordance with the fully low Mach number case and $\widetilde{p}$ is continuous at $\alpha = L$.

Finally, we remark that Eq. (4.5) can be seen as

$$\mathfrak{P}_0(\widetilde{p}_\alpha) + \alpha \times (\varepsilon_{11}\widetilde{p}_\alpha + \varepsilon_0) = 0.$$

Given $p \in (\widetilde{p}_s, \widetilde{p}_e^+)$, this can be seen as an implicit function for α. It reads

$$\alpha(p) = -\frac{\mathfrak{P}_0(p)}{\varepsilon_{11}p + \varepsilon_0}.$$

C Proof of the inequality $F_L < F_\#$

We recall that $F_\#$ is defined by (4.4). For $\phi \in (0, +\infty)$, by squaring the inequality, we obtain

$$\begin{aligned} F_L(\phi) \le F_-(\phi) \qquad &\iff \qquad 0 \le \sqrt{1 + \frac{2\phi}{\Upsilon - 1}} \le 1 + 2\sqrt{\frac{\phi}{2\Upsilon - 1}} \\ &\iff \qquad \sqrt{\phi} \le 2(\Upsilon - 1)\sqrt{2\Upsilon - 1}. \end{aligned}$$

Hence, for $\widetilde{\Phi} \le \frac{\Upsilon-1}{\Upsilon}\sqrt{2\Upsilon - 1} < 2(\Upsilon - 1)\sqrt{2\Upsilon - 1}$, we have $F_L(\widetilde{\Phi}) < F_-(\widetilde{\Phi})$.

Let us show that $F_L(\phi) < F_+(\phi)$ for $\phi \in \left(\frac{\Upsilon-1}{\Upsilon}\sqrt{2\Upsilon - 1}, +\infty\right)$. To do so, we introduce the function

$$f(x) = \frac{\Upsilon - 1}{\Upsilon}\left(1 + \sqrt{1 + \frac{\phi}{(\Upsilon - 1)x}}\right)x$$

so that $F_L(\phi) = f\left(\frac{1}{2}\right)$ and $F_+(\phi) = f\left(\frac{2\Upsilon-1}{3\Upsilon-1}\right)$. f increases over $(0, +\infty)$ and, for $\Upsilon > 1$, we have $\frac{1}{2} < \frac{2\Upsilon-1}{3\Upsilon-1}$ which ends the proof.

Acknowledgments

This work was supported by LRC MANON[7] which is a joint laboratory between CEA DEN/DANS/DM2S and Sorbonne Universités UPMC & CNRS, UMR 7598 (LJLL).

References

[1] R. Abgrall and S. Karni. Computations of compressible multifluids. *J. Comput. Phys.*, 169(2):594–623, 2001.

[2] A. Ambroso, C. Chalons, F. Coquel, T. Galié, E. Godlewski, F. Lagoutière, P.-A. Raviart, and N. Seguin. Numerical coupling of two-phase flows. In *Proceedings of the 2nd International Conference on Scientific Computing and Partial Differential Equations (SCPDE)*, pages 168–178, Hong-Kong, 2005.

[7] www.ljll.math.upmc.fr/groupes/cea/LRC/.

[3] A. Ambroso, C. Chalons, F. Coquel, E. Godlewski, F. Lagoutiere, P.-A. Raviart, N. Seguin, and J.-M. Hérard. Coupling of multiphase flow models. In *Proceedings of the Eleventh International Meeting on Nuclear Thermal-Hydraulics (NURETH)*, 2005.

[4] M. Bernard, S. Dellacherie, G. Faccanoni, B. Grec, O. Lafitte, T.-T. Nguyen, and Y. Penel. Study of a low Mach nuclear core model for single-phase flows. In *ESAIM Proc.*, volume 38, pages 118–134. CEMRACS'11, 2012.

[5] M. Bernard, S. Dellacherie, G. Faccanoni, B. Grec, and Y. Penel. Study of a low Mach nuclear core model for two-phase flows with phase transition I: stiffened gas law. 2013 (submitted).

[6] V. Casulli and D. Greenspan. Pressure method for the numerical solution of transient, compressible fluid flows. *Internat. J. Numer. Methods Fluids*, 4(11):1001–1012, 1984.

[7] C. Chalons, M. Girardin, and S. Kokh. Low-Mach number limit and all-speed Lagrange-Projection scheme for the gaz dynamics equations. 2014.

[8] G.-Q. Chen and D. Wang. The Cauchy problem for the Euler equations for compressible fluids. *Handbook of Mathematical Fluid Dynamics*, 1:421–543, 2002.

[9] I.-L. Chern and Y.-C. Shu. A coupling interface method for elliptic interface problems. *J. Comput. Phys.*, 225(2):2138–2174, 2007.

[10] E.A. Coddington and N. Levinson. *Theory of ordinary differential equations*. New York: McGraw-Hill, 1955.

[11] P. Colella and K. Pao. A projection method for low speed flows. *J. Comput. Phys.*, 149(2):245–269, 1999.

[12] S. Dellacherie. On a diphasic low Mach number system. *ESAIM Math. Model. Numer. Anal.*, 39(3):487–514, 2005.

[13] S. Dellacherie. Analysis of Godunov type schemes applied to the compressible Euler system at low Mach number. *J. Comput. Phys.*, 229(4):978–1016, 2010.

[14] S. Dellacherie. Discretization of boundary conditions and source terms in a compressible nuclear core model at low Mach number. 2014 (in preparation).

[15] B. Desjardins, E. Grenier, P.-L. Lions, and N. Masmoudi. Incompressible limit for solutions of the isentropic Navier–Stokes equations with Dirichlet boundary conditions. *J. Math. Pures Appl.*, 78(5):461–471, 1999.

[16] P. Embid, J. Goodman, and A. Majda. Multiple steady states for 1-D transonic flow. *SIAM J. Sci. Stat. Comput.*, 5(1):21–41, 1984.

[17] M. Gander, L. Halpern, C. Japhet, and V. Martin. Advection diffusion problems with pure advection approximation in subregions. In *Domain decomposition methods in science and engineering XVI*, pages 239–246. Springer, 2007.

[18] F. Gastaldi, A. Quarteroni, and G. Sacchi Landriani. Coupling of two-dimensional hyperbolic and elliptic equations. *Comput. Methods Appl. Mech. Engrg.*, 80(1):347–354, 1990.

[19] E. Godlewski and P.-A. Raviart. The numerical interface coupling of nonlinear hyperbolic systems of conservation laws: I. The scalar case. *Numer. Math.*, 97(1):81–130, 2004.

[20] E. Godlewski and P.-A. Raviart. The numerical interface coupling of nonlinear hyperbolic systems of conservation laws: II. The case of systems. *ESAIM Math. Model. Numer. Anal.*, 39(4):649–692, 2005.

[21] H. Guillard and A. Murrone. On the behavior of upwind schemes in the low Mach number limit: II. Godunov type schemes. *Comput. & Fluids*, 33(4):655–675, 2004.

[22] H. Guillard and C. Viozat. On the behaviour of upwind schemes in the low Mach number limit. *Comput. & Fluids*, 28(1):63–86, 1999.

[23] F. Harlow and J. Welch. Numerical calculation of time-dependent viscous incompressible flow of fluid with free surface. *Phys. Fluids*, 8:2182, 1965.

[24] J.-M. Hérard and O. Hurisse. Coupling two and one-dimensional unsteady Euler equations through a thin interface. *Comput. & Fluids*, 36(4):651–666, 2007.

[25] P. Jenny and B. Müller. Convergence acceleration for computing steady-state compressible flow at low Mach numbers. *Comput. & Fluids*, 28(8):951–972, 1999.

[26] K.C. Karki and S.V. Patankar. Pressure based calculation procedure for viscous flows at all speeds in arbitrary configurations. *AIAA J.*, 27(9):1167–1174, 1989.

[27] S. Klainerman and A. Majda. Singular limits of quasilinear hyperbolic systems with large parameters and the incompressible limit of compressible fluids. *Commun. Pure Appl. Math.*, 34(4):481–524, 1981.

[28] S. Klainerman and A. Majda. Compressible and incompressible fluids. *Commun. Pure Appl. Math.*, 35(5):629–651, 1982.

[29] R. Klein. Semi-implicit extension of a Godunov-type scheme based on low Mach number asymptotics I: one-dimensional flow. *J. Comput. Phys.*, 121(2):213–237, 1995.

[30] K. Knopp. *Theory of functions*, volume 2. Dover Publications (New York), 1947.

[31] W. J. Layton, F. Schieweck, and I. Yotov. Coupling fluid flow with porous media flow. *SIAM J. Numer. Anal.*, 40(6):2195–2218, 2002.

[32] A. Majda and K.G. Lamb. Simplified equations for low Mach number combustion with strong heat release. *IMA Vol. Math. Appl.*, 35:167–211, 1991.

[33] A. Majda and J. Sethian. The derivation and numerical solution of the equations for zero Mach number combustion. *Combust. Sci. Technol.*, 42(3-4):185–205, 1985.

[34] M. Marden. *Geometry of polynomials*. AMS Bookstore, 1966.

[35] C. Merkle and Y.-H. Choi. Computation of low-speed compressible flows with time-marching procedures. *Internat. J. Numer. Methods Engrg.*, 25(2):293–311, 1988.

[36] M. Mu and J. Xu. A two-grid method of a mixed Stokes-Darcy model for coupling fluid flow with porous media flow. *SIAM J. Numer. Anal.*, 45(5):1801–1813, 2007.

[37] C.-D. Munz, S. Roller, R. Klein, and K. Geratz. The extension of incompressible flow solvers to the weakly compressible regime. *Comput. & Fluids*, 32(2):173–196, 2003.

[38] H. Paillere, C. Viozat, A. Kumbaro, and I. Toumi. Comparison of low Mach number models for natural convection problems. *Heat Mass Transf.*, 36(6):567–573, 2000.

[39] S. Paolucci. On the filtering of sound from the Navier-Stokes equations. Technical Report SAND82-8257, Sandia National Laboratories, Dec. 1982.

[40] Y. Penel. An explicit stable numerical scheme for the 1d transport equation. *Discrete Contin. Dyn. Syst. Ser. S*, 5(3):641–656, 2012.

[41] A. Quarteroni and A. Valli. *Domain decomposition methods for partial differential equations*, volume 10. Clarendon Press Oxford, 1999.

[42] S. Schochet. Fast singular limits of hyperbolic PDEs. *J. Differential Equations*, 114(2):476–512, 1994.

[43] S. Schochet. The mathematical theory of low Mach number flows. *ESAIM Math. Model. Numer. Anal.*, 39:441–458, 2005.

[44] D. Serre. *Systems of Conservation Laws 1: Hyperbolicity, entropies, shock waves*, volume 1. Cambridge University Press, 1999.

[45] G.I. Sivashinsky. Hydrodynamic theory of flame propagation in an enclosed volume. *Acta Astronaut.*, 6(5):631–645, 1979.

[46] E.F. Toro. *Riemann solvers and numerical methods for fluid dynamics: a practical introduction.* Springer, 2009.

[47] E. Turkel. Review of preconditioning methods for fluid dynamics. *Appl. Numer. Math.*, 12(1):257–284, 1993.

[48] G. Volpe. Performance of compressible flow codes at low Mach numbers. *AIAA J.*, 31(1):49–56, 1993.